The impact of human-induced climate change on future tornado intensity as revealed through multi-scale modeling

Matthew Woods[1], Robert Trapp[1], and Holly M. Mallinson[2]

[1]UIUC
[2]University of Illinois Urbana-Champaign

June 8, 2023

Abstract

A novel, multi-scale climate modeling approach is used to show the potential for increases in future tornado intensity due to anthropogenic climate change. Historical warm- and cool-season (WARM and COOL) tornado events are virtually placed in a globally warmed future via the "pseudo-global warming" method. As hypothesized based on meteorological arguments, the tornadic-storm and associated vortex of the COOL event experiences consistent and robust increases in intensity, and size in an ensemble of imposed climate-change experiments. The tornadic-storm and associated vortex of the WARM event experiences increases in intensity in some of the experiments, but the response is neither consistent nor robust, and is overall weaker than in the COOL event. An examination of environmental parameters provides further support of the disproportionately stronger response in the cool-season event. These results have implications on future tornadoes forming outside of climatologically favored seasons.

The impact of human-induced climate change on future tornado intensity as revealed through multi-scale modeling

Matthew J. Woods[1]†, Robert J. Trapp[2], and Holly M. Mallinson[3]

[1]Department of Atmospheric Sciences, University of Illinois.
[2]Department of Atmospheric Sciences, University of Illinois.
[3]Department of Atmospheric Sciences, University of Illinois.

Corresponding author: Robert J. Trapp (jtrapp@illinois.edu)
†Current affiliation: National Weather Service, Las Vegas, NV.

Key Points:

- The effects of climate change on tornado intensity have been unclear.
- A novel, multi-modeling approach is used to address such effects.
- The intensity of cool-season tornadoes would appear to be most susceptible.

Abstract

A novel, multi-scale climate modeling approach is used to show the potential for increases in future tornado intensity due to anthropogenic climate change. Historical warm- and cool-season (WARM and COOL) tornado events are virtually placed in a globally warmed future via the "pseudo-global warming" method. As hypothesized based on meteorological arguments, the tornadic-storm and associated vortex of the COOL event experiences consistent and robust increases in intensity, and size in an ensemble of imposed climate-change experiments. The tornadic-storm and associated vortex of the WARM event experiences increases in intensity in some of the experiments, but the response is neither consistent nor robust, and is overall weaker than in the COOL event. An examination of environmental parameters provides further support of the disproportionately stronger response in the cool-season event. These results have implications on future tornadoes forming outside of climatologically favored seasons.

1 Introduction

Hazardous convective weather (HCW) in the form of damaging winds, hail, and tornadoes poses a serious threat to life and property in the United States. From 2012 to 2022, 99 HCW events each produced over $1 billion (inflation-adjusted) in damages (NOAA, 2022). The frequency of these billion-dollar events has increased markedly since the start of the 21st century, owing in part to increased exposure and population density (Strader et al., 2017), but also potentially to anthropogenic climate change (ACC).

HCW depends on the 3D characteristics of environmental temperature, humidity, and wind, which appear to have changed over the last few decades (Gensini & Brooks, 2018; Tang et al. 2019; Taszarek et al., 2021) and are projected to change further by the late 21st century under ACC. For example, as shown by Trapp et al. (2007), warming and humidification of lower-tropospheric air yields increases in convective available potential energy (CAPE), which leads to increases in the potential intensity of convective-storm updrafts. Conversely, relatively more warming at high latitudes weakens the meridional temperature gradient and thus weakens the vertical shear of the horizontal wind (hereinafter, VWS) per the thermal wind relation (e.g., Trapp et al. 2007); this suggests a reduction in the tendency for convective updrafts to develop significant, long-lived rotational cores. General circulation model (GCM) and regional climate model (RCM) simulations reveal decreases in VWS that are disproportionately smaller than increases in CAPE, indicating an increase in frequency and/or intensity of future HCW events under ACC in the United States (e.g., Trapp et al., 2007; Del Genio et al., 2007; Trapp et al., 2009; Diffenbaugh et al., 2013; Gensini et al., 2014; Seeley & Romps, 2015; Hoogewind et al., 2017). Of relevance herein is the seasonal non-uniformity to this increase: Boreal winter tends to exhibit the largest relative increase in the CAPE–VWS covariate (Diffenbaugh et al., 2013). This is consistent with historical trends of environmental parameters computed using reanalysis data (Gensini & Brooks, 2018).

Precisely how these conclusions relate to *tornado intensity*, and thus address the very basic question of whether the environmental conditions due to 21st century ACC will contribute to more intense tornadoes, is unclear. This is partly because relationships between observed tornado intensity and environmental parameters such as CAPE and VWS are ambiguous. For example, although nonzero CAPE is considered a necessary condition for, and thus critically relevant to tornadic-storm formation, CAPE alone does not correlate well with observed tornado intensity (Thompson et al., 2012). As supported by our analyses in section 3.3, a possible link could be made using multivariate environmental parameters such as the significant tornado parameter (STP), which appears to better discriminate environments of significant tornadoes from those of nonsignificant tornadoes (Thompson et al., 2012), although still not perfectly. However, an environment-only argument has a critical limitation, namely, that realization of a significant tornado is conditional on tornadic-storm initiation, which STP does not unambiguously predict. Indeed, the mean frequency of storms that initiate given a supportive environment is non-uniform in time and space, and even appears to change under late 21st century ACC (Hoogewind et al., 2017).

Explicit climate modeling of tornadoes is an alternative to the use of environmental parameters and removes the storm-initiation limitation. Although such an approach has been computationally prohibitive because of the small-scale of tornadoes (~100 m to 1 km), multi-scale modeling now offers a tractable solution. Herein we follow Trapp & Hoogewind (2016) and employ the pseudo global warming (PGW) method (Schär et al., 1996; Frei et al., 1998; Kimura and Kitoh, 2007; Sato et al., 2007) using a novel, multi-scale, multi-model approach. Briefly, the PGW method involves a comparison of simulations of events under their true 4D environment (the control; CTRL) with those under a 4D environment modified by a climate-change perturbation representative of *mean atmospheric conditions* over future (here, late 21st century) and historical (here, late 20th century) time slices. Thus, this method allows for an isolation of the response of an event to an imposed environment of the future. Because *event-level* PGW applications (see Trapp et al., 2021) involve relatively short time integrations, they also allow for the use of higher resolution and multiple realizations.

Two archetypal yet regionally and seasonally contrasting events are considered. The first is the 10 February 2013 (hereinafter, COOL) event that includes the EF-4 tornado in Hattiesburg, Mississippi, and the second is the 20 May 2013 (hereinafter, WARM) event that includes the EF-5 tornado in Moore, Oklahoma. Together, these tornadoes were responsible for 24 fatalities, more than 300 injuries, and approximately $2 billion in damage (NOAA, 2013). Our working hypothesis is that the WARM event will exhibit relatively less intensity changes under PGW than the COOL event.

Analyses of these event simulations provide the initial means to address this hypothesis. However, the spatio-temporal representations of the tornadic storms, and even the total numbers of storms, are different between the PGW and CTRL simulations (see Fig. 1). This implied lack of a clear CTRL–to–PGW comparison of *specific* tornadic storms means that a quantitative evaluation of the climate change effect on the intensity of *specific* tornadoes is tenuous. Accordingly, we introduce an additional step wherein an idealized numerical model is integrated using initial and boundary conditions (ic/bc) drawn from the regional-model simulations. The relatively reduced complexity and higher spatial resolutions afforded by this idealized-modeling implementation of the PGW methodology helps further isolate the climate change response on a single storm, and allows for explicit diagnoses of tornado intensity.

2 Materials and Methods

2.1 PGW

The PGW method involves simulations of some event wherein its actual, present-day forcing is modified through the addition of a climate-change perturbation or "delta", which is the difference between mean conditions over future and historical time slices during a relevant month. Separate sets of deltas are constructed using historical and Representative Concentration Pathway 8.5 simulations from each of five GCMs (GFDL-CM3, MIROC5, NCAR-CCSM4, IPSL-CM5A-LR, and NorESM-1M). The GCM data originate from the Coupled Model Intercomparison Project phase 5 (Taylor et al., 2012), and provide a range of convective-storm environments over historical and future time periods (e.g., see Diffenbaugh et al., 2013; Seeley & Romps, 2015).

Three different formulations of the climate-change deltas (see Trapp et al., 2021), computed using five different GCMs, provide an ensemble of 15 simulations plus an additional composite-delta simulation to assess the PGW response of each event. Because these 16 different deltas explicitly represent a range in the climate-change signal, we argue that their use toward generation of an ensemble is more relevant than other approaches. Specifically, and importantly, we are interested in the model response to the imposed future climate change and associated ic/bc rather than in the model response to variations in parameterization schemes, etc.

2.2 Regional model configuration

The CTRL and PGW simulations of the WARM and COOL events are performed using version 4.0 of the Weather Research and Forecasting model (WRF) (Skamarock et al., 2008). The parent computational domains have horizontal grid spacings of 3 km. Subdomains of 1-km grid spacing are nested within the parent domains over central Oklahoma and central Mississippi, respectively (Fig. S1). The results reported in section 3.1 are based on analyses over the nested domains.

The simulations are initialized at 12 UTC for both events. This allows for more than six hours of "spin-up" time prior to the observed EF-5 Moore (~2000 UTC) and EF-4 Hattiesburg (~2300 UTC) tornadoes, which is typical for weather-event simulations with WRF (Skamarock, 2004). Initial and boundary conditions are derived from the North American Mesoscale Forecast System analysis. Additional details regarding the WRF configuration can be found in Trapp et al. (2021). Decisions on the configuration and on the ultimate veracity of the CTRL simulations were established by comparing model output from configuration-sensitivity experiments to observed radar characteristics and tornado reports, as described in Woods (2021).

Tornadoes are not resolved on model grids with 1-km spacings. However, as demonstrated in the Supplement, their signatures and potential intensity can be inferred using vertical vorticity (VV) computed at 80 m AGL, which is approximately the height of the first level above the lower boundary of the model. A VV value locally exceeding 7.5×10^{-3} s^{-1}, which is the 99th percentile of gridpoint values in the CTRL simulation, serves as a tornado proxy occurrence. A VV value exceeding 1.25×10^{-2} s^{-1}, which is the 99.9th percentile, serves as a significant tornado proxy occurrence. Coexistence of local updraft velocities exceeding 5 m s^{-1} is also required, to ensure that the VV is associated with a convective updraft. Differentiating tornado intensity based on VV is justified in the Supplement through an analyses of a vortex model, and also follows from Doppler radar-based studies by Toth et al. (2012) and others.

2.3 Idealized model configuration

The idealized simulations are performed using Cloud Model 1 (CM1) (Bryan & Fritsch, 2002). Grid stretching is employed such that the horizontal grid spacing is 64 m over the inner 80 x 80 km of the 180 x 180 x 18.5 km model domain, and then increased to 2.5 km at the domain edges. Vertical grid spacing varies from 20 m in the lowest model levels to 250 m in the upper levels. Additional details regarding the CM1 model configuration can be found in Woods (2021). Note that the actual tornadoes that occurred on 20 May 2013 and 10 February 2013 had damage widths of 1600 m and 1200 m, respectively. Even if the core diameters of maximum winds of these tornadoes were 50% of these widths, the cores would still be represented by ~10 grid points. So, although our simulations do not have grid spacings appropriate to resolve fine-scale structures of the tornadoes, the simulations are certainly sufficient to represent core widths and windspeeds, which is one goal of these simulations.

The initial and boundary conditions are drawn from the WRF output of the CTRL and PGW simulations. Specifically, 60 x 60 km horizontal averages centered about the WRF grid point nearest to Moore, Oklahoma and Hattiesburg, Mississippi are used to obtain vertical profiles at 20 UTC 20 May 2013 and 23 UTC 10 February, respectively, which represent the pre-tornadic conditions during these two events. A single deep convective storm is initiated within these environments via updraft nudging (Naylor & Gilmore, 2012) that persisted for 20 minutes. Our analysis of the subsequent tornadic circulations begins at 30 min, i.e., 10 min after the cessation of the nudging.

Tornadic-like vortices (TLVs) are identified by examining near-surface fields of windspeed, VV, and the Obuko-Weiss (OW) parameter. Adapting the approaches of Sherburn & Parker (2019), Gray & Frame (2021), and others, TLV identification requires VV, windspeed, and OW to exceed 0.1 s^{-1}, 30 m s^{-1}, and 0.03 s^{-2}, respectively, and be collocated with low-level updraft speeds exceeding 5 m s^{-1}. Upon locating the strongest TLV, maximum and minimum of x-direction and y-direction wind components are found within 500 m of the vortex center. The locations of these maxima and minima are used to determine an average radius (r) of maximum winds (V).

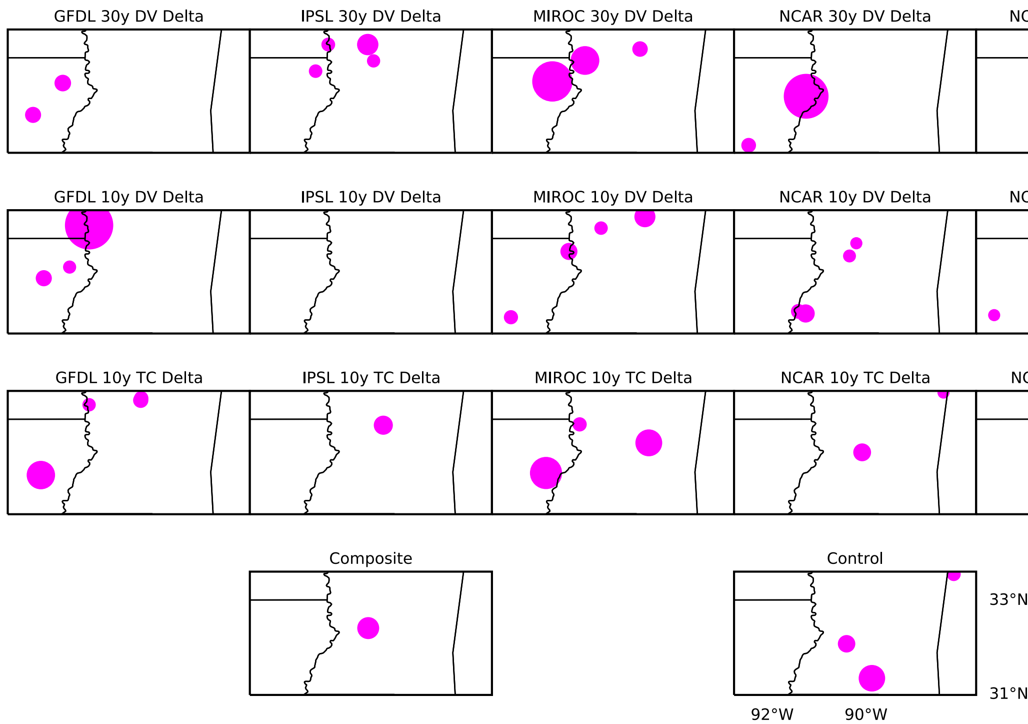

Figure 1. Locations of tornado proxies (magenta dots) for the regional-modeling simulations of the WARM event during the hour ending 2100 UTC (upper panels), and COOL event during the hour ending 2230 UTC (lower panels). The size of the dots correspond nonlinearly to the VV associated with the proxy. The subpanels indicate the individual experiments composing the ensemble.

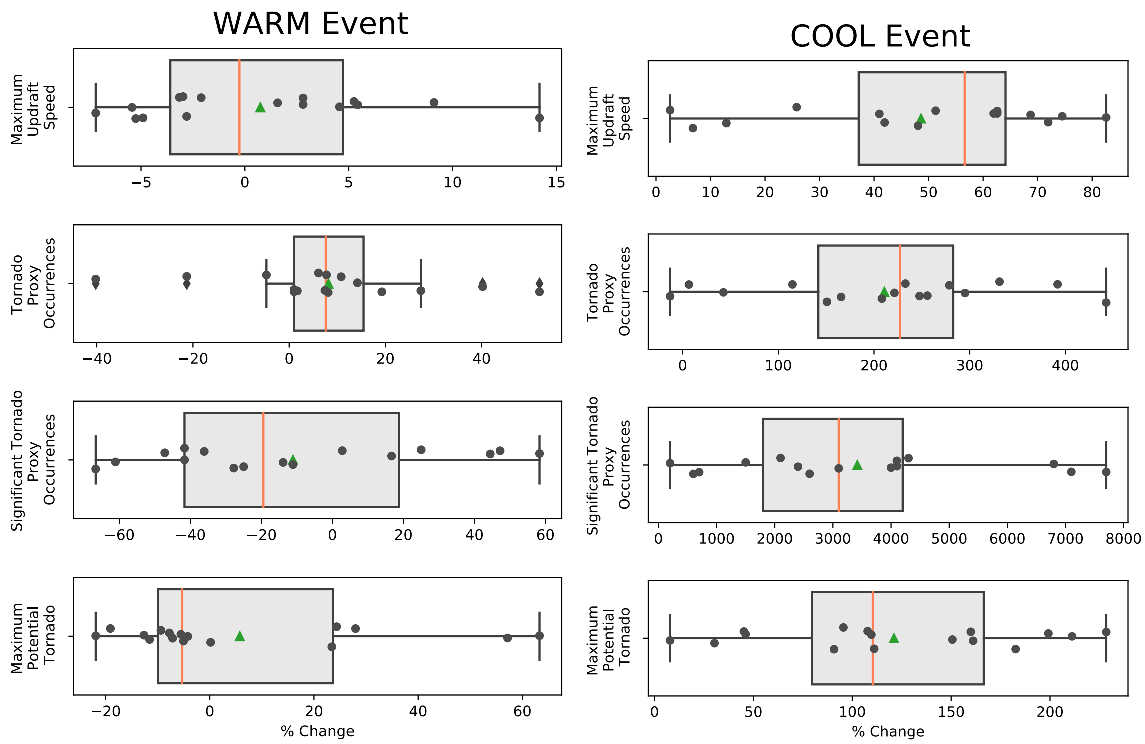

Figure 2. Box-and-whisker plots of tornadic-storm intensity metrics, as evaluated from the regional modeling simulations of the WARM event (left) and COOL event (right). Values of these metrics are given as percentage changes in the PGW simulations relative to the CTRL simulation. The median is the orange line, mean is the green triangle, and individual data points are the black circles.

3 Results

3.1 Regional-modeling perspective

An ensemble of 16 simulations is used to assess the PGW response of each event. The ensemble members represent a range of possible future realizations of the event. Herein, if 75% of the ensemble members exhibit the same sign in the percentage change (PGW relative to CTRL) in a given metric, we consider the PGW response for that metric to be *consistent*. If we equate the signal in the metric to the mean value across the ensemble, and the noise to the standard deviation, the response in this metric is considered to be *robust* (*highly robust*) if the PGW signal-to-noise ratio in a given metric exceeds one (two) (e.g., Diffenbaugh et al., 2013).

We begin with two metrics that provide information on overall storm intensity. The first is the cumulative gridpoint exceedance of 55 dBZ simulated radar reflectivity (Figs. S2 and S3). This metric quantifies the total area of intense convective storms over a given simulation. A consistent, robust response is shown in this metric, as represented by a mean percentage increase of +110% (PGW exceedances relative to those in the CTRL) (Fig. S3). Thus, the PGW-modified conditions resulted in relatively more extensive and intense convective storms in association with the WARM event.

Cumulative gridpoint exceedances of simulated updraft speed confirm this increase in the extent of intense convective storms under PGW (Figs. S3 and S4); a consistent, robust response is represented by a mean percentage increase of +40%. The *peak* updraft speeds are comparatively stronger in only half of the PGW simulations, with a mean percentage increase of +1% (Fig. 2). These results indicate that intense convective updrafts in a late 21st century realization of the WARM event would be more numerous or larger, but not always stronger.

The PGW response in occurrences of our tornado proxy is consistent albeit not robust, with a mean percentage increase of 8% (Fig. 2). The mean response occurrences of our significant tornado proxy is neither consistent nor robust, with a mean percentage decrease of -11% (Fig. 2). Finally, the peak VV per PGW simulation, which provides some information about the *potential* tornado intensity, is also neither consistent nor robust, with a mean percentage increase of 5% (and median percentage decrease of -5%) (Fig. 2). Thus, the regional modeling suggests relatively more but not necessarily stronger tornadic circulations in a late 21st century realization the WARM event, albeit with large uncertainty (see also Fig. 1).

Like the WARM event, the COOL event under PGW also tends to be characterized by more intense convective storms. Specifically, cumulative gridpoint exceedances of simulated reflectivity of 55 dBZ are greater in all but one of the PGW simulations, thus contributing to an average percentage increase of +125%, and a consistent and robust response in this metric (Figs. S2 and S3). The other metric for overall storm intensity, cumulative gridpoint exceedances of updraft speed of 25 m s^{-1}, is consistent but not robust; notably, the average percentage increase in such strong updraft occurrence in the COOL event is +712%, as compared to the +40% increase associated with the WARM event (see Figs. S2 and S3). *All* PGW simulations had peak updraft speeds exceeding the 31 m s^{-1} peak of the CTRL (Fig. 2), thus implying a consistent and robust response. Moreover, half of the PGW simulations had peak updrafts exceeding 50 m s^{-1}, which historically are speeds more readily supportive in warm-season, Great Plains environments than in cool-season, southeast U.S. environments. These results indicate that intense convective updrafts in a late 21st century realization of the COOL event would be more numerous *and* stronger.

Occurrences of the tornado proxy are substantially greater under PGW in many of the simulations, leading to a mean percentage increase relative to CTRL of +211% (Fig. 2). Occurrences of the significant tornado proxy are also substantially greater, with a mean percentage increase of +3244%, in this consistent and robust response (Fig. 2). Finally, a consistent and robust response is indicated in the peak VV per PGW simulation, and thus potential tornado intensity, with an average percentage increase of +121% (Fig. 2).

Collectively, these results suggest that tornadic circulations in a late 21st century realization of the COOL event would be more numerous and stronger. In agreement with our hypothesis, the magnitude of the response of this archetypal cool-season event to PGW is much larger than that of the archetypal warm-season event; this finding is also in agreement with Bercos-Hickey et al. (2021). There is still ambiguity, however, in precisely how the analyzed response relates to tornado intensity, given both the model grid resolution and the nature of the tornado proxy. Thus, we now use the TLV–resolving idealized PGW simulations to compute explicit measures of tornado intensity, and thus help clarify the regional-model results.

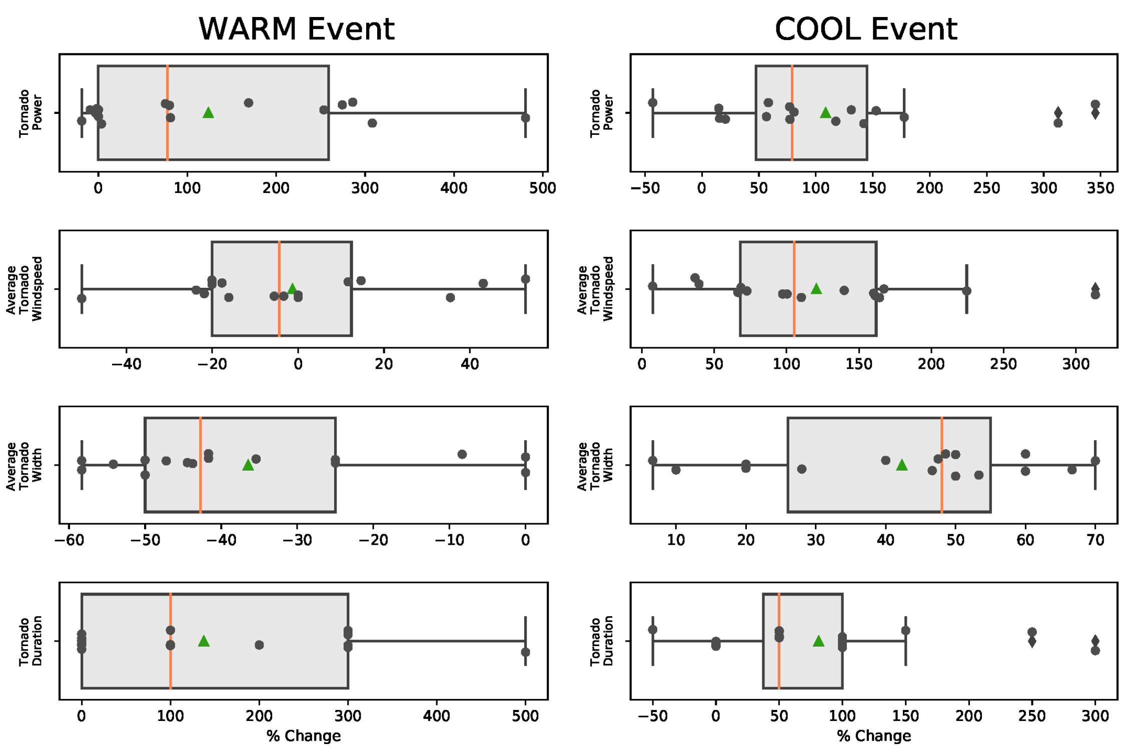

Figure 3. As in Figure 2, except for tornado intensity metrics (see text).

3.2 Idealized modeling perspective

The idealized PGW simulations have steady, horizontally homogeneous initial and boundary conditions that were drawn from the regional-model simulations of the WARM and COOL events (Figs. S5-S6). The much finer grid spacings (64 m) allow for explicit quantifications of TLVs that form within the simulated storms. For this we use *tornado power*, which accounts for the tornadic wind speed as well as the width and length of the tornado track. As adapted from Fricker et al. (2014), instantaneous tornado power can be calculated as

$$P = \pi r^2 \rho V^3 \qquad (1)$$

where r represents the average radius of maximum winds, ρ is the air density (assumed to be 1 kg m^{-3}), and V is the average maximum surface wind speed at radius r. Total tornado power here is the summation of $\log(P)$ over the lifetime of the tornado-like vortex,

$$P_t = \sum \log(P) \qquad (2)$$

In simulations of the WARM event, the PGW response in total power is neither consistent nor robust. However, the 16-member ensemble contributed to a mean percentage increase in P_t of +124% (Fig. 3). This percentage increase is due to a few experiments with relatively stronger vortex windspeeds; none of the experiments exhibited wider vortices (Fig. 3). Thus, as in the coarser-resolution regional modeling simulations, there are indications of intensity increases in this violent, Great Plains, warm-season tornado given an imposed climate change, but with large uncertainty.

For the COOL event, the PGW response in total power is both consistent and robust, with an average percentage increase of +109% (Fig. 3). The increases in P_t are driven by consistent and robust increases in tornadic-vortex strength and width (Fig. 3). The relatively longer duration of the tornadic vortices (+81%) also contribute to the larger P_t under PGW. These high-resolution simulations are in agreement with the regional modeling simulations, and clearly demonstrate an increased intensity and duration for this archetypal cool-season tornado given an imposed climate change. The collective simulations also confirm our hypothesis regarding a relatively larger response of this cool-season event.

Table 1. Mean values, and percentage changes relative to the CTRL experiment, of environmental parameters computed from the initial/boundary conditions of the idealized-modeling PGW experiments.

Event	CAPE (J/kg)		CIN (J/kg)		LCL (m)		SRH3 (m2/s2)		SRH1 (m2/s2)		S06 (m/s)		STP	
WARM	4484	+56	0	+100	1774	+23	86	-58	34	-53	24	-14	0.2	-72
COOL	1037	+162	-24	-61	243	+33	427	-21	327	-23	36	-4	2.2	+100

CIN is convective inhibition; LCL is lifting condensation level; SRH3 is storm-relative environmental helicity, evaluated over the 0-3 km layer; SRH1 is storm-relative environmental helicity, evaluated over the 0-1 km layer; S06 is the bulk wind shear, evaluated over the 0-6 km layer.

We can use the ic/bc of the idealized experiments to explore the meteorological arguments on which this hypothesis is based. The mean, PGW-enhanced CAPE of 4484 J kg^{-1} and 1037 J kg^{-1} for the WARM and COOL events, respectively, represent consistent and robust increases of +56% and +162% relative to the corresponding CTRL environments (Table 1). The mean, PGW-diminished VWS of 24 m s^{-1} and 36 m s^{-1} for the WARM and COOL events, respectively, represent consistent and robust decreases of -14% and -4% relative to the corresponding CTRL environments (Table 1); disproportionate decreases of storm-relative helicity, another measure of VWS, are also revealed for the WARM versus COOL events (-53% and -23%, respectively; Table 1). When these and other environmental parameters are combined through the multivariate parameter STP, the environment of the WARM event is found to be relatively *less* supportive of a significant tornado under PGW (mean percentage decrease of -72%), while the environment of the COOL event is relatively *more* supportive under PGW (mean percentage increase of +100%) (Table 1).

3.3 Generality of the conclusions

Although the intensity changes described herein apply to the specific WARM and COOL events simulated, all potential tornadic-storm events realized during the warm- and cool-season months of consideration would be subject to the same range of climate-change perturbations. To help quantify how these perturbations alone might contribute to environments of significant tornadoes, STP is calculated at all points within the regional-model domain for the CTRL and PGW simulations of both events (Fig. S7). The PGW – CTRL difference for each PGW ensemble member represents the contribution of the monthly climate change perturbation for that member (see section 2.1) to the STP change. Upon spatially averaging the PGW – CTRL differences, we find that the ensemble mean STP perturbation is -0.30 for the month of May, and +0.70 for the month of February. The implication is that ACC would contribute, *on average*, to environments that are relatively *less* supportive of a significant tornado during May across the central Great Plains U.S., and relatively *more* supportive of a significant tornado during February across the southeast U.S. Such environmental changes have been noted in studies by Gensini & Brooks (2018), Bercos-Hickey et al. (2021), and Lepore et al. (2021).

4 Summary and Conclusions

Evidence for the potential of ACC to lead to increases in future tornado intensity is provided through a novel climate modeling study of two contemporary, archetypal, warm- and cool-season tornado events. The tornadic-storm and associated vortex of the cool-season event experiences a consistent and robust increase in intensity and size when virtually placed in a globally warmed future via the PGW method. The tornadic-storm and associated vortex of the warm-season event experiences increases in intensity in some of the virtual experiments, but the response is neither consistent nor robust, and is overall weaker than in the cool-season event. Consideration of other data lends support to such a disproportionate response based on season of the year.

The preceding statement should not be interpreted to mean that *all* tornadoes will be stronger in the future. The atmospheric heterogeneity arising from naturally variable large-scale atmospheric circulations, high-frequency weather systems, convective storms and their residual effects, and land-surface variations (e.g., see Trapp, 2013) will continue to create diverse environmental conditions both supportive and non-supportive of thunderstorm formation. Significant tornadogenesis within such thunderstorms will also continue to require a delicate balance between VWS and CAPE, among other environmental parameters. Yet because cool-season environments in the current climate tend to be characterized by very large VWS and small CAPE, future increases in CAPE (decreases in VWS) due to ACC appear to be relatively more conductive to (less impactful on) this balance and thus on cool-season tornado potential.

These findings have implications on the possible impacts of future tornadoes forming outside of climatologically favored seasons, in the United States and elsewhere around the world. Indeed, situational awareness of tornado risk tends to be reduced during seasons such as boreal winter, which offers one explanation for high fatalities from tornadic events during these times (e.g., Ashley, 2007). It follows that more intense future tornadoes would have the potential to result in more fatalities and damage.

Acknowledgments

This research was supported by the National Science Foundation, award AGS 1923042. The WRF simulations were conducted on the NCAR Cheyenne Computing Facility. The CM1 simulations were conducted on the Blue Waters Petascale Computing Facility. We thank Dr. George Bryan for making available and otherwise supporting the CM1 model. We acknowledge the World Climate Research Programme's Working Group on Coupled Modelling, which is responsible for CMIP, and we thank the climate modeling groups indicated in section 2.1 for producing and making available their model output.

Open Research

The following GCM data sets used in this study are available through the CMIP5 repository (https://esgf-node.llnl.gov/projects/cmip5/), using these criteria: Models: GFDL-CM3, MIROC5, NCAR-CCSM4, IPSL-CM5A-LR, and NorESM-1M; Experiments: historical and RCP8.5; Ensemble: r1i1p1; Realm: atmos; and Time Frequency: 3hr or 6hr. The WRF model is available at https://www2.mmm.ucar.edu/wrf/users/, and the CM1 model is available at https://www2.mmm.ucar.edu/people/bryan/cm1/. Relevant simulation data are available through the Illinois Data Bank at https://databank.illinois.edu/datasets/IDB-4479773 .

References

Ashley, W. S. (2007). Spatial and Temporal Analysis of Tornado Fatalities in the United States: 1880–2005. *Weather and Forecasting*, *22*(6), 1214–1228. https://doi.org/10.1175/2007WAF2007004.1

Bercos-Hickey, E., Patricola, C. M., & Gallus, W. A. (2021). Anthropogenic Influences on Tornadic Storms. *Journal of Climate*, 1–57. https://doi.org/10.1175/JCLI-D-20-0901.1

Bryan, G. H., & Fritsch, J. M. (2002). A Benchmark Simulation for Moist Nonhydrostatic Numerical Models. *Monthly Weather Review*, *130*(12), 2917–2928. https://doi.org/10.1175/1520-0493(2002)130<2917:ABSFMN>2.0.CO;2

Del Genio, A. D., Yao, M.-S., & Jonas, J. (2007). Will moist convection be stronger in a warmer climate? *Geophysical Research Letters*, *34*(16). https://doi.org/10.1029/2007GL030525

Diffenbaugh, N. S., Scherer, M., & Trapp, R. J. (2013). Robust increases in severe thunderstorm environments in response to greenhouse forcing. *Proceedings of the National Academy of Sciences*. https://doi.org/10.1073/pnas.1307758110

Frei, C., Schär, C., Lüthi, D., & Davies, H. C. (1998). Heavy precipitation processes in a warmer climate. *Geophysical Research Letters*, *25*(9), 1431–1434. https://doi.org/10.1029/98GL51099

Fricker, T., Elsner, J. B., Camp, P., & Jagger, T. H. (2014). Empirical estimates of kinetic energy from some recent U.S. tornadoes. *Geophysical Research Letters*. https://doi.org/10.1002/2014GL060441

Gensini, V. A., & Brooks, H. E. (2018). Spatial trends in United States tornado frequency. *Npj Climate and Atmospheric Science 2018 1:1*, *1*(1), 1–5. https://doi.org/10.1038/s41612-018-0048-2

Gensini, V. A., Ramseyer, C., & Mote, T. L. (2014). Future convective environments using NARCCAP. *International Journal of Climatology*, *34*(5), 1699–1705. https://doi.org/10.1002/joc.3769

Gray, K., & Frame, J. (2021). The impact of midlevel shear orientation on the longevity of and downdraft location and tornado-like vortex formation within simulated supercells. Monthly Weather Review, 149, 3739-3759, https://doi.org/10.1175/MWR-D-21-0085.1

Hoogewind, K. A., Baldwin, M. E., & Trapp, R. J. (2017). The Impact of Climate Change on Hazardous Convective Weather in the United States: Insight from High-Resolution Dynamical Downscaling. *Journal of Climate*, *30*, 10081–10100. https://doi.org/10.1175/JCLI-D-16-0885.1

Kimura, F., & Kitoh, A. (2007). *Downscaling by pseudo global warming method. In Final report to the ICCAP.* Kyoto, Japan.

Lepore, C., Abernathey, R., Henderson, N., Allen, J. T., & Tippett, M. K. (2021). Future Global Convective Environments in CMIP6 Models. *Earth's Future*, e2021EF002277. https://doi.org/https://doi.org/10.1029/2021EF002277

Naylor, J., & Gilmore, M. S. (2012). Convective Initiation in an Idealized Cloud Model Using an Updraft Nudging Technique. *Monthly Weather Review*, *140*(11), 3699–3705. https://doi.org/10.1175/MWR-D-12-00163.1

NOAA. (2013). NCEI Storm Events Database. Retrieved from https://www.ncdc.noaa.gov/stormevents/

NOAA. (2022). NOAA National Centers for Environmental Information (NCEI) U.S. Billion-Dollar Weather and Climate Disasters (2022). https://doi.org/10.25921/stkw-7w73

Sato, T., Kimura, F., & Kitoh, A. (2007). Projection of global warming onto regional precipitation over Mongolia using a regional climate model. *Journal of Hydrology*, *333*(1), 144–154. https://doi.org/https://doi.org/10.1016/j.jhydrol.2006.07.023

Schär, C., Frei, C., Lüthi, D., & Davies, H. C. (1996). Surrogate climate-change scenarios for regional climate models. *Geophysical Research Letters*, *23*(6), 669–672. https://doi.org/10.1029/96GL00265

Seeley, J. T., & Romps, D. M. (2015). The Effect of Global Warming on Severe Thunderstorms in the United States. *Journal of Climate*, *28*(6), 2443–2458. https://doi.org/10.1175/JCLI-D-14-00382.1

Sherburn, K. D., & Parker, M. D. (2019). The development of severe vortices within simulated high-shear, low-CAPE convection. *Monthly Weather Review*. https://doi.org/10.1175/MWR-D-18-0246.1

Skamarock, W. C., Klemp, J. B., Dudhia, J., Gill, D. O., Barker, D. M., Huang, X.-Y., et al. (2008). *A description of the Advanced Research WRF version 3*. *NCAR Tech. Note TN-475+STR*.

Skamarock, W. C. (2004). Evaluating Mesoscale NWP Models Using Kinetic Energy Spectra. *Monthly Weather Review*, *132*(12), 3019–3032. https://doi.org/10.1175/MWR2830.1

Strader, S. M., Ashley, W. S., Pingel, T. J., & Krmenec, A. J. (2017). Projected 21st century changes in tornado exposure, risk, and disaster potential. *Climatic Change*, *141*(2), 301–313. https://doi.org/10.1007/s10584-017-1905-4

Tang, B. J., Gensini, V. A., & Homeyer, C. R. (2019). Trends in United States large hail environments and observations. *Npj Climate and Atmospheric Science,* https://doi.org/10.1038/s41612-019-0103-7

Taylor, K. E., Stouffer, R. J., & Meehl, G. A. (2012). An Overview of CMIP5 and the Experiment Design. *Bulletin of the American Meteorological Society*, *93*(4), 485–498. https://doi.org/10.1175/BAMS-D-11-00094.1

Taszarek, M., Allen, J. T., Marchio, M., & Brooks, H. E. (2021). Global climatology and trends in convective environments from ERA5 and rawinsonde data. *Npj Climate and Atmospheric Science,* https://doi.org/10.1038/s41612-021-00190-x

Thompson, R. L., Smith, B. T., Grams, J. S., Dean, A. R., & Broyles, C. (2012). Convective Modes for Significant Severe Thunderstorms in the Contiguous United States. Part II: Supercell and QLCS Tornado Environments. *Weather and Forecasting*, *27*(5), 1136–1154. https://doi.org/10.1175/WAF-D-11-00116.1

Toth, M., Trapp, R. J., Wurman, J., & Kosiba, K. A. (2012). Comparison of Mobile-Radar Measurements of Tornado Intensity with Corresponding WSR-88D Measurements. *Weather and Forecasting*, *28*(2), 418–426. https://doi.org/10.1175/WAF-D-12-00019.1

Trapp, R. J. (2013). *Mesoscale-Convective Processes in the Atmosphere*. Cambridge University Press.

Trapp, R. J., & Hoogewind, K. A. (2016). The realization of extreme tornadic storm events under future anthropogenic climate change. *Journal of Climate*. https://doi.org/10.1175/JCLI-D-15-0623.1

Trapp, R.J., Woods, M. J., Lasher-Trapp, S. G., & Grover, M. A. (2021). Alternative Implementations of the “Pseudo-Global-Warming” Methodology for Event-Based Simulations. *Journal of Geophysical Research: Atmospheres*, *126*(24). https://doi.org/10.1029/2021JD035017

Trapp, R. J, Diffenbaugh, N. S., Brooks, H. E., Baldwin, M. E., Robinson, E. D., & Pal, J. S. (2007). Changes in severe thunderstorm environment frequency during the 21st century caused by anthropogenically enhanced global radiative forcing. *Proceedings of the National Academy of Sciences*, *104*(50), 19719–19723. https://doi.org/10.1073/pnas.0705494104

Trapp, R. J., Diffenbaugh, N. S., & Gluhovsky, A. (2009). Transient response of severe thunderstorm forcing to elevated greenhouse gas concentrations. *Geophysical Research Letters*, *36*(1), L01703. https://doi.org/10.1029/2008GL036203

Woods, M. J. (2021). *Understanding extreme tornado events under future climate change through the pseudo-global warming methodology*. University of Illinois at Urbana-Champaign.

The impact of human-induced climate change on future tornado intensity as revealed through multi-scale modeling

Matthew J. Woods[1]†, Robert J. Trapp[2], and Holly M. Mallinson[3]

[1]Department of Atmospheric Sciences, University of Illinois.
[2]Department of Atmospheric Sciences, University of Illinois.
[3]Department of Atmospheric Sciences, University of Illinois.

Corresponding author: Robert J. Trapp (jtrapp@illinois.edu)
†Current affiliation: National Weather Service, Las Vegas, NV.

Key Points:

- The effects of climate change on tornado intensity have been unclear.
- A novel, multi-modeling approach is used to address such effects.
- The intensity of cool-season tornadoes would appear to be most susceptible.

Abstract

A novel, multi-scale climate modeling approach is used to show the potential for increases in future tornado intensity due to anthropogenic climate change. Historical warm- and cool-season (WARM and COOL) tornado events are virtually placed in a globally warmed future via the "pseudo-global warming" method. As hypothesized based on meteorological arguments, the tornadic-storm and associated vortex of the COOL event experiences consistent and robust increases in intensity, and size in an ensemble of imposed climate-change experiments. The tornadic-storm and associated vortex of the WARM event experiences increases in intensity in some of the experiments, but the response is neither consistent nor robust, and is overall weaker than in the COOL event. An examination of environmental parameters provides further support of the disproportionately stronger response in the cool-season event. These results have implications on future tornadoes forming outside of climatologically favored seasons.

1 Introduction

Hazardous convective weather (HCW) in the form of damaging winds, hail, and tornadoes poses a serious threat to life and property in the United States. From 2012 to 2022, 99 HCW events each produced over $1 billion (inflation-adjusted) in damages (NOAA, 2022). The frequency of these billion-dollar events has increased markedly since the start of the 21st century, owing in part to increased exposure and population density (Strader et al., 2017), but also potentially to anthropogenic climate change (ACC).

HCW depends on the 3D characteristics of environmental temperature, humidity, and wind, which appear to have changed over the last few decades (Gensini & Brooks, 2018; Tang et al. 2019; Taszarek et al., 2021) and are projected to change further by the late 21st century under ACC. For example, as shown by Trapp et al. (2007), warming and humidification of lower-tropospheric air yields increases in convective available potential energy (CAPE), which leads to increases in the potential intensity of convective-storm updrafts. Conversely, relatively more warming at high latitudes weakens the meridional temperature gradient and thus weakens the vertical shear of the horizontal wind (hereinafter, VWS) per the thermal wind relation (e.g., Trapp et al. 2007); this suggests a reduction in the tendency for convective updrafts to develop significant, long-lived rotational cores. General circulation model (GCM) and regional climate model (RCM) simulations reveal decreases in VWS that are disproportionately smaller than increases in CAPE, indicating an increase in frequency and/or intensity of future HCW events under ACC in the United States (e.g., Trapp et al., 2007; Del Genio et al., 2007; Trapp et al., 2009; Diffenbaugh et al., 2013; Gensini et al., 2014; Seeley & Romps, 2015; Hoogewind et al., 2017). Of relevance herein is the seasonal non-uniformity to this increase: Boreal winter tends to exhibit the largest relative increase in the CAPE–VWS covariate (Diffenbaugh et al., 2013). This is consistent with historical trends of environmental parameters computed using reanalysis data (Gensini & Brooks, 2018).

Precisely how these conclusions relate to *tornado intensity*, and thus address the very basic question of whether the environmental conditions due to 21st century ACC will contribute to more intense tornadoes, is unclear. This is partly because relationships between observed tornado intensity and environmental parameters such as CAPE and VWS are ambiguous. For example, although nonzero CAPE is considered a necessary condition for, and thus critically relevant to tornadic-storm formation, CAPE alone does not correlate well with observed tornado intensity (Thompson et al., 2012). As supported by our analyses in section 3.3, a possible link could be made using multivariate environmental parameters such as the significant tornado parameter (STP), which appears to better discriminate environments of significant tornadoes from those of nonsignificant tornadoes (Thompson et al., 2012), although still not perfectly. However, an environment-only argument has a critical limitation, namely, that realization of a significant tornado is conditional on tornadic-storm initiation, which STP does not unambiguously predict. Indeed, the mean frequency of storms that initiate given a supportive environment is non-uniform in time and space, and even appears to change under late 21st century ACC (Hoogewind et al., 2017).

Explicit climate modeling of tornadoes is an alternative to the use of environmental parameters and removes the storm-initiation limitation. Although such an approach has been computationally prohibitive because of the small-scale of tornadoes (~100 m to 1 km), multi-scale modeling now offers a tractable solution. Herein we follow Trapp & Hoogewind (2016) and employ the pseudo global warming (PGW) method (Schär et al., 1996; Frei et al., 1998; Kimura and Kitoh, 2007; Sato et al., 2007) using a novel, multi-scale, multi-model approach. Briefly, the PGW method involves a comparison of simulations of events under their true 4D environment (the control; CTRL) with those under a 4D environment modified by a climate-change perturbation representative of *mean atmospheric conditions* over future (here, late 21st century) and historical (here, late 20th century) time slices. Thus, this method allows for an isolation of the response of an event to an imposed environment of the future. Because *event-level* PGW applications (see Trapp et al., 2021) involve relatively short time integrations, they also allow for the use of higher resolution and multiple realizations.

Two archetypal yet regionally and seasonally contrasting events are considered. The first is the 10 February 2013 (hereinafter, COOL) event that includes the EF-4 tornado in Hattiesburg, Mississippi, and the second is the 20 May 2013 (hereinafter, WARM) event that includes the EF-5 tornado in Moore, Oklahoma. Together, these tornadoes were responsible for 24 fatalities, more than 300 injuries, and approximately $2 billion in damage (NOAA, 2013). Our working hypothesis is that the WARM event will exhibit relatively less intensity changes under PGW than the COOL event.

Analyses of these event simulations provide the initial means to address this hypothesis. However, the spatio-temporal representations of the tornadic storms, and even the total numbers of storms, are different between the PGW and CTRL simulations (see Fig. 1). This implied lack of a clear CTRL–to–PGW comparison of *specific* tornadic storms means that a quantitative evaluation of the climate change effect on the intensity of *specific* tornadoes is tenuous. Accordingly, we introduce an additional step wherein an idealized numerical model is integrated using initial and boundary conditions (ic/bc) drawn from the regional-model simulations. The relatively reduced complexity and higher spatial resolutions afforded by this idealized-modeling implementation of the PGW methodology helps further isolate the climate change response on a single storm, and allows for explicit diagnoses of tornado intensity.

2 Materials and Methods

2.1 PGW

The PGW method involves simulations of some event wherein its actual, present-day forcing is modified through the addition of a climate-change perturbation or “delta”, which is the difference between mean conditions over future and historical time slices during a relevant month. Separate sets of deltas are constructed using historical and Representative Concentration Pathway 8.5 simulations from each of five GCMs (GFDL-CM3, MIROC5, NCAR-CCSM4, IPSL-CM5A-LR, and NorESM-1M). The GCM data originate from the Coupled Model Intercomparison Project phase 5 (Taylor et al., 2012), and provide a range of convective-storm environments over historical and future time periods (e.g., see Diffenbaugh et al., 2013; Seeley & Romps, 2015).

Three different formulations of the climate-change deltas (see Trapp et al., 2021), computed using five different GCMs, provide an ensemble of 15 simulations plus an additional composite-delta simulation to assess the PGW response of each event. Because these 16 different deltas explicitly represent a range in the climate-change signal, we argue that their use toward generation of an ensemble is more relevant than other approaches. Specifically, and importantly, we are interested in the model response to the imposed future climate change and associated ic/bc rather than in the model response to variations in parameterization schemes, etc.

2.2 Regional model configuration

The CTRL and PGW simulations of the WARM and COOL events are performed using version 4.0 of the Weather Research and Forecasting model (WRF) (Skamarock et al., 2008). The parent computational domains have horizontal grid spacings of 3 km. Subdomains of 1-km grid spacing are nested within the parent domains over central Oklahoma and central Mississippi, respectively (Fig. S1). The results reported in section 3.1 are based on analyses over the nested domains.

The simulations are initialized at 12 UTC for both events. This allows for more than six hours of "spin-up" time prior to the observed EF-5 Moore (~2000 UTC) and EF-4 Hattiesburg (~2300 UTC) tornadoes, which is typical for weather-event simulations with WRF (Skamarock, 2004). Initial and boundary conditions are derived from the North American Mesoscale Forecast System analysis. Additional details regarding the WRF configuration can be found in Trapp et al. (2021). Decisions on the configuration and on the ultimate veracity of the CTRL simulations were established by comparing model output from configuration-sensitivity experiments to observed radar characteristics and tornado reports, as described in Woods (2021).

Tornadoes are not resolved on model grids with 1-km spacings. However, as demonstrated in the Supplement, their signatures and potential intensity can be inferred using vertical vorticity (VV) computed at 80 m AGL, which is approximately the height of the first level above the lower boundary of the model. A VV value locally exceeding 7.5×10^{-3} s^{-1}, which is the 99th percentile of gridpoint values in the CTRL simulation, serves as a tornado proxy occurrence. A VV value exceeding 1.25×10^{-2} s^{-1}, which is the 99.9th percentile, serves as a significant tornado proxy occurrence. Coexistence of local updraft velocities exceeding 5 m s^{-1} is also required, to ensure that the VV is associated with a convective updraft. Differentiating tornado intensity based on VV is justified in the Supplement through an analyses of a vortex model, and also follows from Doppler radar-based studies by Toth et al. (2012) and others.

2.3 Idealized model configuration

The idealized simulations are performed using Cloud Model 1 (CM1) (Bryan & Fritsch, 2002). Grid stretching is employed such that the horizontal grid spacing is 64 m over the inner 80 x 80 km of the 180 x 180 x 18.5 km model domain, and then increased to 2.5 km at the domain edges. Vertical grid spacing varies from 20 m in the lowest model levels to 250 m in the upper levels. Additional details regarding the CM1 model configuration can be found in Woods (2021). Note that the actual tornadoes that occurred on 20 May 2013 and 10 February 2013 had damage widths of 1600 m and 1200 m, respectively. Even if the core diameters of maximum winds of these tornadoes were 50% of these widths, the cores would still be represented by ~10 grid points. So, although our simulations do not have grid spacings appropriate to resolve fine-scale structures of the tornadoes, the simulations are certainly sufficient to represent core widths and windspeeds, which is one goal of these simulations.

The initial and boundary conditions are drawn from the WRF output of the CTRL and PGW simulations. Specifically, 60 x 60 km horizontal averages centered about the WRF grid point nearest to Moore, Oklahoma and Hattiesburg, Mississippi are used to obtain vertical profiles at 20 UTC 20 May 2013 and 23 UTC 10 February, respectively, which represent the pre-tornadic conditions during these two events. A single deep convective storm is initiated within these environments via updraft nudging (Naylor & Gilmore, 2012) that persisted for 20 minutes. Our analysis of the subsequent tornadic circulations begins at 30 min, i.e., 10 min after the cessation of the nudging.

Tornadic-like vortices (TLVs) are identified by examining near-surface fields of windspeed, VV, and the Obuko-Weiss (OW) parameter. Adapting the approaches of Sherburn & Parker (2019), Gray & Frame (2021), and others, TLV identification requires VV, windspeed, and OW to exceed 0.1 s^{-1}, 30 m s^{-1}, and 0.03 s^{-2}, respectively, and be collocated with low-level updraft speeds exceeding 5 m s^{-1}. Upon locating the strongest TLV, maximum and minimum of *x*-direction and *y*-direction wind components are found within 500 m of the vortex center. The locations of these maxima and minima are used to determine an average radius (r) of maximum winds (V).

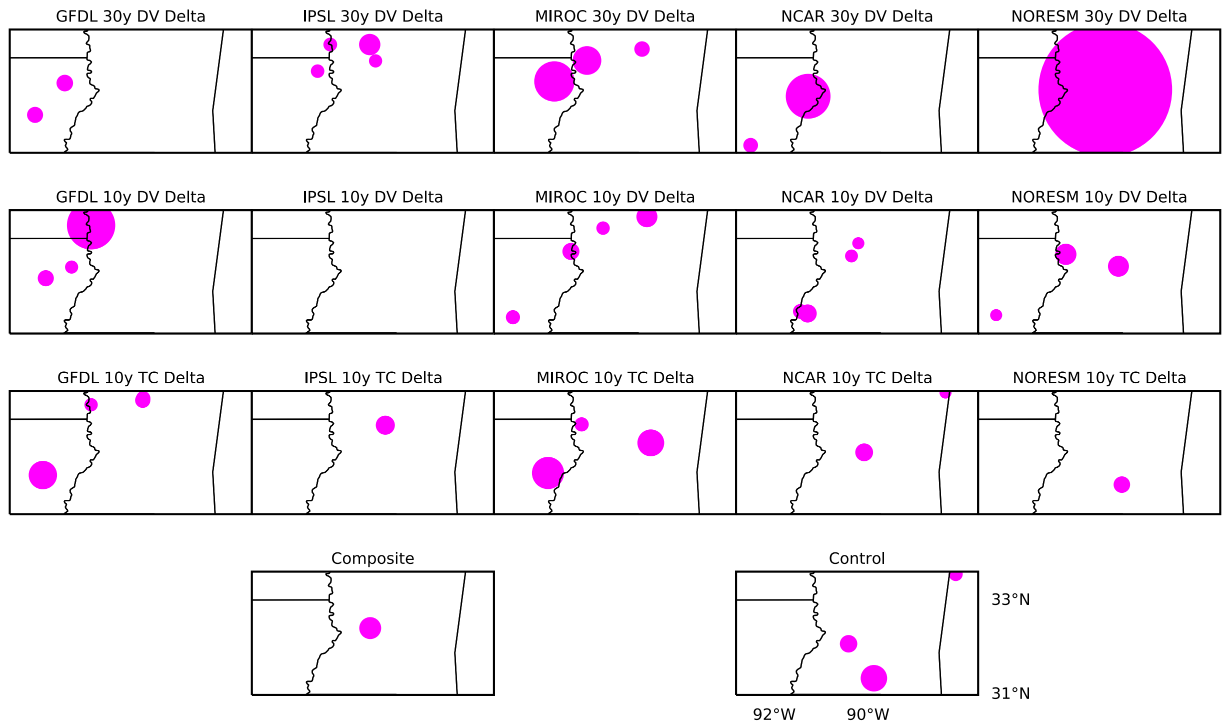

Figure 1. Locations of tornado proxies (magenta dots) for the regional-modeling simulations of the WARM event during the hour ending 2100 UTC (upper panels), and COOL event during the hour ending 2230 UTC (lower panels). The size of the dots correspond nonlinearly to the VV associated with the proxy. The subpanels indicate the individual experiments composing the ensemble.

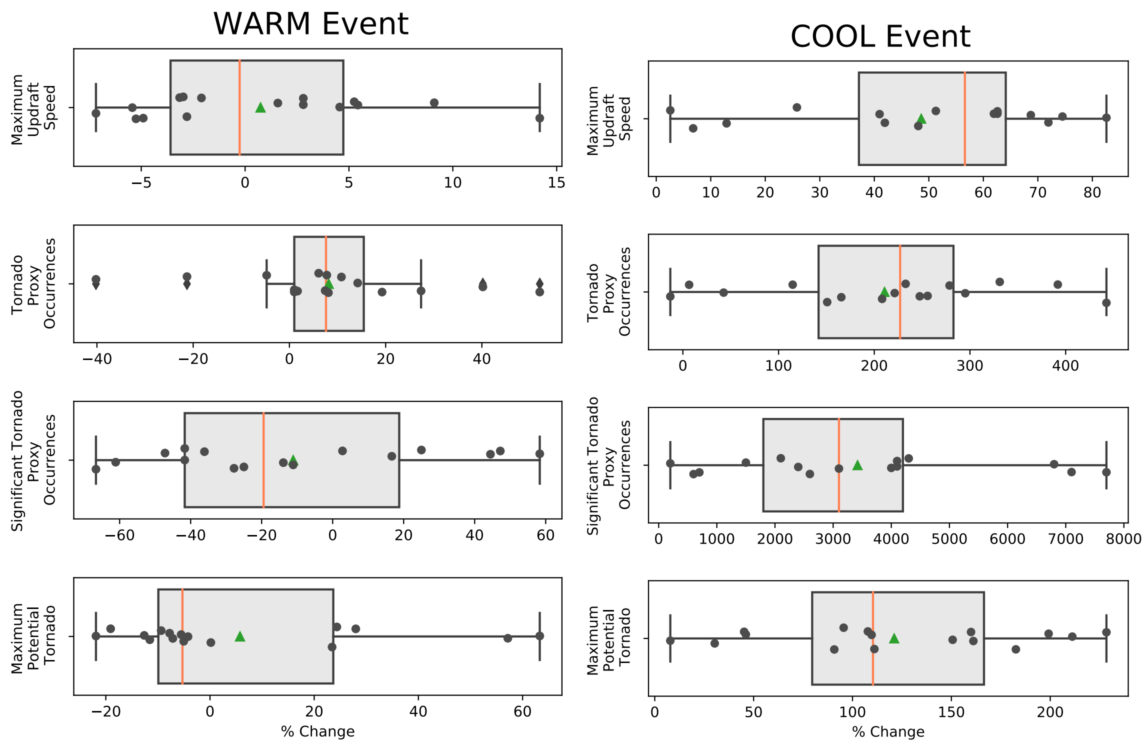

Figure 2. Box-and-whisker plots of tornadic-storm intensity metrics, as evaluated from the regional modeling simulations of the WARM event (left) and COOL event (right). Values of these metrics are given as percentage changes in the PGW simulations relative to the CTRL simulation. The median is the orange line, mean is the green triangle, and individual data points are the black circles.

3 Results

3.1 Regional-modeling perspective

An ensemble of 16 simulations is used to assess the PGW response of each event. The ensemble members represent a range of possible future realizations of the event. Herein, if 75% of the ensemble members exhibit the same sign in the percentage change (PGW relative to CTRL) in a given metric, we consider the PGW response for that metric to be *consistent*. If we equate the signal in the metric to the mean value across the ensemble, and the noise to the standard deviation, the response in this metric is considered to be *robust* (*highly robust*) if the PGW signal-to-noise ratio in a given metric exceeds one (two) (e.g., Diffenbaugh et al., 2013).

We begin with two metrics that provide information on overall storm intensity. The first is the cumulative gridpoint exceedance of 55 dBZ simulated radar reflectivity (Figs. S2 and S3). This metric quantifies the total area of intense convective storms over a given simulation. A consistent, robust response is shown in this metric, as represented by a mean percentage increase of +110% (PGW exceedances relative to those in the CTRL) (Fig. S3). Thus, the PGW-modified conditions resulted in relatively more extensive and intense convective storms in association with the WARM event.

Cumulative gridpoint exceedances of simulated updraft speed confirm this increase in the extent of intense convective storms under PGW (Figs. S3 and S4); a consistent, robust response is represented by a mean percentage increase of +40%. The *peak* updraft speeds are comparatively stronger in only half of the PGW simulations, with a mean percentage increase of +1% (Fig. 2). These results indicate that intense convective updrafts in a late 21st century realization of the WARM event would be more numerous or larger, but not always stronger.

The PGW response in occurrences of our tornado proxy is consistent albeit not robust, with a mean percentage increase of 8% (Fig. 2). The mean response occurrences of our significant tornado proxy is neither consistent nor robust, with a mean percentage decrease of -11% (Fig. 2). Finally, the peak VV per PGW simulation, which provides some information about the *potential* tornado intensity, is also neither consistent nor robust, with a mean percentage increase of 5% (and median percentage decrease of -5%) (Fig. 2). Thus, the regional modeling suggests relatively more but not necessarily stronger tornadic circulations in a late 21st century realization the WARM event, albeit with large uncertainty (see also Fig. 1).

Like the WARM event, the COOL event under PGW also tends to be characterized by more intense convective storms. Specifically, cumulative gridpoint exceedances of simulated reflectivity of 55 dBZ are greater in all but one of the PGW simulations, thus contributing to an average percentage increase of +125%, and a consistent and robust response in this metric (Figs. S2 and S3). The other metric for overall storm intensity, cumulative gridpoint exceedances of updraft speed of 25 m s^{-1}, is consistent but not robust; notably, the average percentage increase in such strong updraft occurrence in the COOL event is +712%, as compared to the +40% increase associated with the WARM event (see Figs. S2 and S3). *All* PGW simulations had peak updraft speeds exceeding the 31 m s^{-1} peak of the CTRL (Fig. 2), thus implying a consistent and robust response. Moreover, half of the PGW simulations had peak updrafts exceeding 50 m s^{-1}, which historically are speeds more readily supportive in warm-season, Great Plains environments than in cool-season, southeast U.S. environments. These results indicate that intense convective updrafts in a late 21st century realization of the COOL event would be more numerous *and* stronger.

Occurrences of the tornado proxy are substantially greater under PGW in many of the simulations, leading to a mean percentage increase relative to CTRL of +211% (Fig. 2). Occurrences of the significant tornado proxy are also substantially greater, with a mean percentage increase of +3244%, in this consistent and robust response (Fig. 2). Finally, a consistent and robust response is indicated in the peak VV per PGW simulation, and thus potential tornado intensity, with an average percentage increase of +121% (Fig. 2).

Collectively, these results suggest that tornadic circulations in a late 21st century realization of the COOL event would be more numerous and stronger. In agreement with our hypothesis, the magnitude of the response of this archetypal cool-season event to PGW is much larger than that of the archetypal warm-season event; this finding is also in agreement with Bercos-Hickey et al. (2021). There is still ambiguity, however, in precisely how the analyzed response relates to tornado intensity, given both the model grid resolution and the nature of the tornado proxy. Thus, we now use the TLV–resolving idealized PGW simulations to compute explicit measures of tornado intensity, and thus help clarify the regional-model results.

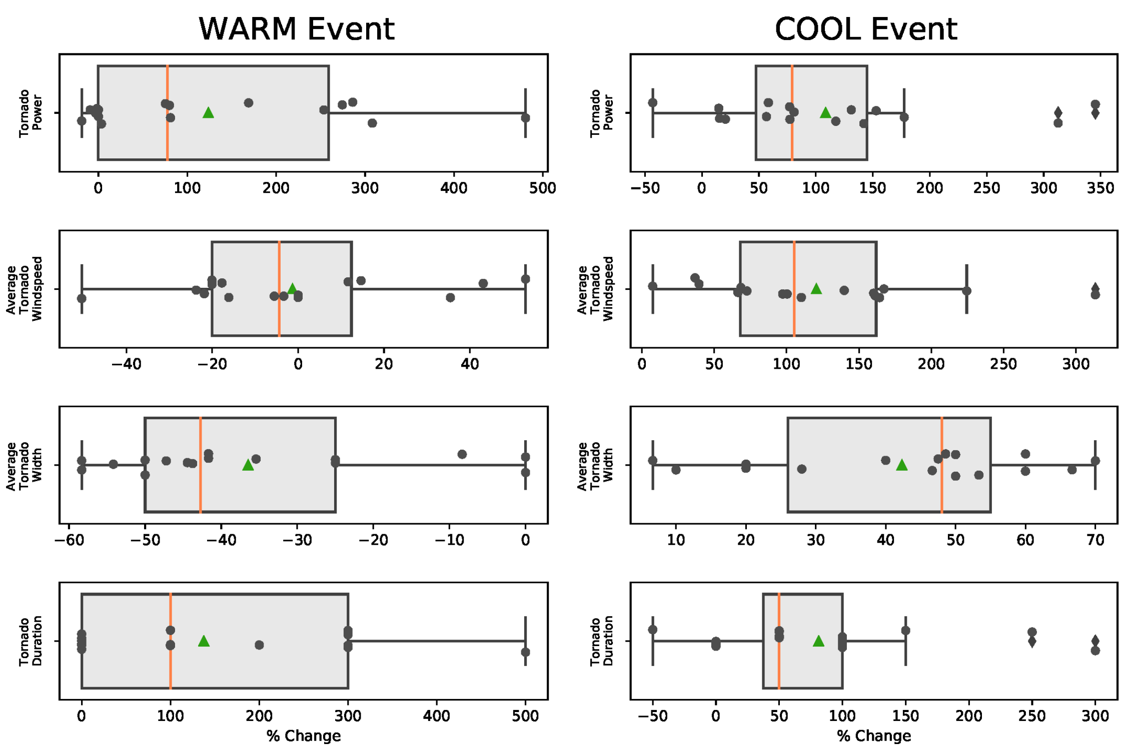

Figure 3. As in Figure 2, except for tornado intensity metrics (see text).

3.2 Idealized modeling perspective

The idealized PGW simulations have steady, horizontally homogeneous initial and boundary conditions that were drawn from the regional-model simulations of the WARM and COOL events (Figs. S5-S6). The much finer grid spacings (64 m) allow for explicit quantifications of TLVs that form within the simulated storms. For this we use *tornado power*, which accounts for the tornadic wind speed as well as the width and length of the tornado track. As adapted from Fricker et al. (2014), instantaneous tornado power can be calculated as

$$P = \pi r^2 \rho V^3 \qquad (1)$$

where r represents the average radius of maximum winds, ρ is the air density (assumed to be 1 kg m^{-3}), and V is the average maximum surface wind speed at radius r. Total tornado power here is the summation of $\log(P)$ over the lifetime of the tornado-like vortex,

$$P_t = \sum \log(P) \qquad (2)$$

In simulations of the WARM event, the PGW response in total power is neither consistent nor robust. However, the 16-member ensemble contributed to a mean percentage increase in P_t of +124% (Fig. 3). This percentage increase is due to a few experiments with relatively stronger vortex windspeeds; none of the experiments exhibited wider vortices (Fig. 3). Thus, as in the coarser-resolution regional modeling simulations, there are indications of intensity increases in this violent, Great Plains, warm-season tornado given an imposed climate change, but with large uncertainty.

For the COOL event, the PGW response in total power is both consistent and robust, with an average percentage increase of +109% (Fig. 3). The increases in P_t are driven by consistent and robust increases in tornadic-vortex strength and width (Fig. 3). The relatively longer duration of the tornadic vortices (+81%) also contribute to the larger P_t under PGW. These high-resolution simulations are in agreement with the regional modeling simulations, and clearly demonstrate an increased intensity and duration for this archetypal cool-season tornado given an imposed climate change. The collective simulations also confirm our hypothesis regarding a relatively larger response of this cool-season event.

Table 1. Mean values, and percentage changes relative to the CTRL experiment, of environmental parameters computed from the initial/boundary conditions of the idealized-modeling PGW experiments.

Event	**CAPE (J/kg)**		**CIN (J/kg)**		**LCL (m)**		**SRH3 (m2/s2)**		**SRH1 (m2/s2)**		**S06 (m/s)**		**STP**	
WARM	4484	+56	0	+100	1774	+23	86	-58	34	-53	24	-14	0.2	-72
COOL	1037	+162	-24	-61	243	+33	427	-21	327	-23	36	-4	2.2	+100

CIN is convective inhibition; LCL is lifting condensation level; SRH3 is storm-relative environmental helicity, evaluated over the 0-3 km layer; SRH1 is storm-relative environmental helicity, evaluated over the 0-1 km layer; S06 is the bulk wind shear, evaluated over the 0-6 km layer.

We can use the ic/bc of the idealized experiments to explore the meteorological arguments on which this hypothesis is based. The mean, PGW-enhanced CAPE of 4484 J kg^{-1} and 1037 J kg^{-1} for the WARM and COOL events, respectively, represent consistent and robust increases of +56% and +162% relative to the corresponding CTRL environments (Table 1). The mean, PGW-diminished VWS of 24 m s^{-1} and 36 m s^{-1} for the WARM and COOL events, respectively, represent consistent and robust decreases of -14% and -4% relative to the corresponding CTRL environments (Table 1); disproportionate decreases of storm-relative helicity, another measure of VWS, are also revealed for the WARM versus COOL events (-53% and -23%, respectively; Table 1). When these and other environmental parameters are combined through the multivariate parameter STP, the environment of the WARM event is found to be relatively *less* supportive of a significant tornado under PGW (mean percentage decrease of -72%), while the environment of the COOL event is relatively *more* supportive under PGW (mean percentage increase of +100%) (Table 1).

3.3 Generality of the conclusions

Although the intensity changes described herein apply to the specific WARM and COOL events simulated, all potential tornadic-storm events realized during the warm- and cool-season months of consideration would be subject to the same range of climate-change perturbations. To help quantify how these perturbations alone might contribute to environments of significant tornadoes, STP is calculated at all points within the regional-model domain for the CTRL and PGW simulations of both events (Fig. S7). The PGW – CTRL difference for each PGW ensemble member represents the contribution of the monthly climate change perturbation for that member (see section 2.1) to the STP change. Upon spatially averaging the PGW – CTRL differences, we find that the ensemble mean STP perturbation is -0.30 for the month of May, and +0.70 for the month of February. The implication is that ACC would contribute, *on average*, to environments that are relatively *less* supportive of a significant tornado during May across the central Great Plains U.S., and relatively *more* supportive of a significant tornado during February across the southeast U.S. Such environmental changes have been noted in studies by Gensini & Brooks (2018), Bercos-Hickey et al. (2021), and Lepore et al. (2021).

4 Summary and Conclusions

Evidence for the potential of ACC to lead to increases in future tornado intensity is provided through a novel climate modeling study of two contemporary, archetypal, warm- and cool-season tornado events. The tornadic-storm and associated vortex of the cool-season event experiences a consistent and robust increase in intensity and size when virtually placed in a globally warmed future via the PGW method. The tornadic-storm and associated vortex of the warm-season event experiences increases in intensity in some of the virtual experiments, but the response is neither consistent nor robust, and is overall weaker than in the cool-season event. Consideration of other data lends support to such a disproportionate response based on season of the year.

The preceding statement should not be interpreted to mean that *all* tornadoes will be stronger in the future. The atmospheric heterogeneity arising from naturally variable large-scale atmospheric circulations, high-frequency weather systems, convective storms and their residual effects, and land-surface variations (e.g., see Trapp, 2013) will continue to create diverse environmental conditions both supportive and non-supportive of thunderstorm formation. Significant tornadogenesis within such thunderstorms will also continue to require a delicate balance between VWS and CAPE, among other environmental parameters. Yet because cool-season environments in the current climate tend to be characterized by very large VWS and small CAPE, future increases in CAPE (decreases in VWS) due to ACC appear to be relatively more conductive to (less impactful on) this balance and thus on cool-season tornado potential.

These findings have implications on the possible impacts of future tornadoes forming outside of climatologically favored seasons, in the United States and elsewhere around the world. Indeed, situational awareness of tornado risk tends to be reduced during seasons such as boreal winter, which offers one explanation for high fatalities from tornadic events during these times (e.g., Ashley, 2007). It follows that more intense future tornadoes would have the potential to result in more fatalities and damage.

Acknowledgments

This research was supported by the National Science Foundation, award AGS 1923042. The WRF simulations were conducted on the NCAR Cheyenne Computing Facility. The CM1 simulations were conducted on the Blue Waters Petascale Computing Facility. We thank Dr. George Bryan for making available and otherwise supporting the CM1 model. We acknowledge the World Climate Research Programme's Working Group on Coupled Modelling, which is responsible for CMIP, and we thank the climate modeling groups indicated in section 2.1 for producing and making available their model output.

Open Research

The following GCM data sets used in this study are available through the CMIP5 repository (https://esgf-node.llnl.gov/projects/cmip5/), using these criteria: Models: GFDL-CM3, MIROC5, NCAR-CCSM4, IPSL-CM5A-LR, and NorESM-1M; Experiments: historical and RCP8.5; Ensemble: r1i1p1; Realm: atmos; and Time Frequency: 3hr or 6hr. The WRF model is available at https://www2.mmm.ucar.edu/wrf/users/, and the CM1 model is available at https://www2.mmm.ucar.edu/people/bryan/cm1/. Relevant simulation data are available through the Illinois Data Bank at https://databank.illinois.edu/datasets/IDB-4479773 .

References

Ashley, W. S. (2007). Spatial and Temporal Analysis of Tornado Fatalities in the United States: 1880–2005. *Weather and Forecasting*, *22*(6), 1214–1228. https://doi.org/10.1175/2007WAF2007004.1

Bercos-Hickey, E., Patricola, C. M., & Gallus, W. A. (2021). Anthropogenic Influences on Tornadic Storms. *Journal of Climate*, 1–57. https://doi.org/10.1175/JCLI-D-20-0901.1

Bryan, G. H., & Fritsch, J. M. (2002). A Benchmark Simulation for Moist Nonhydrostatic Numerical Models. *Monthly Weather Review*, *130*(12), 2917–2928. https://doi.org/10.1175/1520-0493(2002)130<2917:ABSFMN>2.0.CO;2

Del Genio, A. D., Yao, M.-S., & Jonas, J. (2007). Will moist convection be stronger in a warmer climate? *Geophysical Research Letters*, *34*(16). https://doi.org/10.1029/2007GL030525

Diffenbaugh, N. S., Scherer, M., & Trapp, R. J. (2013). Robust increases in severe thunderstorm environments in response to greenhouse forcing. *Proceedings of the National Academy of Sciences*. https://doi.org/10.1073/pnas.1307758110

Frei, C., Schär, C., Lüthi, D., & Davies, H. C. (1998). Heavy precipitation processes in a warmer climate. *Geophysical Research Letters*, *25*(9), 1431–1434. https://doi.org/10.1029/98GL51099

Fricker, T., Elsner, J. B., Camp, P., & Jagger, T. H. (2014). Empirical estimates of kinetic energy from some recent U.S. tornadoes. *Geophysical Research Letters*. https://doi.org/10.1002/2014GL060441

Gensini, V. A., & Brooks, H. E. (2018). Spatial trends in United States tornado frequency. *Npj Climate and Atmospheric Science 2018 1:1*, *1*(1), 1–5. https://doi.org/10.1038/s41612-018-0048-2

Gensini, V. A., Ramseyer, C., & Mote, T. L. (2014). Future convective environments using NARCCAP. *International Journal of Climatology*, *34*(5), 1699–1705. https://doi.org/10.1002/joc.3769

Gray, K., & Frame, J. (2021). The impact of midlevel shear orientation on the longevity of and downdraft location and tornado-like vortex formation within simulated supercells. Monthly Weather Review, 149, 3739-3759, https://doi.org/10.1175/MWR-D-21-0085.1

Hoogewind, K. A., Baldwin, M. E., & Trapp, R. J. (2017). The Impact of Climate Change on Hazardous Convective Weather in the United States: Insight from High-Resolution Dynamical Downscaling. *Journal of Climate*, *30*, 10081–10100. https://doi.org/10.1175/JCLI-D-16-0885.1

Kimura, F., & Kitoh, A. (2007). *Downscaling by pseudo global warming method. In Final report to the ICCAP*. Kyoto, Japan.

Lepore, C., Abernathey, R., Henderson, N., Allen, J. T., & Tippett, M. K. (2021). Future Global Convective Environments in CMIP6 Models. *Earth's Future*, e2021EF002277. https://doi.org/https://doi.org/10.1029/2021EF002277

Naylor, J., & Gilmore, M. S. (2012). Convective Initiation in an Idealized Cloud Model Using an Updraft Nudging Technique. *Monthly Weather Review*, *140*(11), 3699–3705. https://doi.org/10.1175/MWR-D-12-00163.1

NOAA. (2013). NCEI Storm Events Database. Retrieved from https://www.ncdc.noaa.gov/stormevents/

NOAA. (2022). NOAA National Centers for Environmental Information (NCEI) U.S. Billion-Dollar Weather and Climate Disasters (2022). https://doi.org/10.25921/stkw-7w73

Sato, T., Kimura, F., & Kitoh, A. (2007). Projection of global warming onto regional precipitation over Mongolia using a regional climate model. *Journal of Hydrology*, *333*(1), 144–154. https://doi.org/https://doi.org/10.1016/j.jhydrol.2006.07.023

Schär, C., Frei, C., Lüthi, D., & Davies, H. C. (1996). Surrogate climate-change scenarios for regional climate models. *Geophysical Research Letters*, *23*(6), 669–672. https://doi.org/10.1029/96GL00265

Seeley, J. T., & Romps, D. M. (2015). The Effect of Global Warming on Severe Thunderstorms in the United States. *Journal of Climate*, *28*(6), 2443–2458. https://doi.org/10.1175/JCLI-D-14-00382.1

Sherburn, K. D., & Parker, M. D. (2019). The development of severe vortices within simulated high-shear, low-CAPE convection. *Monthly Weather Review*. https://doi.org/10.1175/MWR-D-18-0246.1

Skamarock, W. C., Klemp, J. B., Dudhia, J., Gill, D. O., Barker, D. M., Huang, X.-Y., et al. (2008). *A description of the Advanced Research WRF version 3*. *NCAR Tech. Note TN-475+STR*.

Skamarock, W. C. (2004). Evaluating Mesoscale NWP Models Using Kinetic Energy Spectra. *Monthly Weather Review*, *132*(12), 3019–3032. https://doi.org/10.1175/MWR2830.1

Strader, S. M., Ashley, W. S., Pingel, T. J., & Krmenec, A. J. (2017). Projected 21st century changes in tornado exposure, risk, and disaster potential. *Climatic Change*, *141*(2), 301–313. https://doi.org/10.1007/s10584-017-1905-4

Tang, B. J., Gensini, V. A., & Homeyer, C. R. (2019). Trends in United States large hail environments and observations. *Npj Climate and Atmospheric Science,* https://doi.org/10.1038/s41612-019-0103-7

Taylor, K. E., Stouffer, R. J., & Meehl, G. A. (2012). An Overview of CMIP5 and the Experiment Design. *Bulletin of the American Meteorological Society*, *93*(4), 485–498. https://doi.org/10.1175/BAMS-D-11-00094.1

Taszarek, M., Allen, J. T., Marchio, M., & Brooks, H. E. (2021). Global climatology and trends in convective environments from ERA5 and rawinsonde data. *Npj Climate and Atmospheric Science,* https://doi.org/10.1038/s41612-021-00190-x

Thompson, R. L., Smith, B. T., Grams, J. S., Dean, A. R., & Broyles, C. (2012). Convective Modes for Significant Severe Thunderstorms in the Contiguous United States. Part II: Supercell and QLCS Tornado Environments. *Weather and Forecasting*, *27*(5), 1136–1154. https://doi.org/10.1175/WAF-D-11-00116.1

Toth, M., Trapp, R. J., Wurman, J., & Kosiba, K. A. (2012). Comparison of Mobile-Radar Measurements of Tornado Intensity with Corresponding WSR-88D Measurements. *Weather and Forecasting*, *28*(2), 418–426. https://doi.org/10.1175/WAF-D-12-00019.1

Trapp, R. J. (2013). *Mesoscale-Convective Processes in the Atmosphere*. Cambridge University Press.

Trapp, R. J., & Hoogewind, K. A. (2016). The realization of extreme tornadic storm events under future anthropogenic climate change. *Journal of Climate*. https://doi.org/10.1175/JCLI-D-15-0623.1

Trapp, R.J., Woods, M. J., Lasher-Trapp, S. G., & Grover, M. A. (2021). Alternative Implementations of the "Pseudo-Global-Warming" Methodology for Event-Based Simulations. *Journal of Geophysical Research: Atmospheres*, *126*(24). https://doi.org/10.1029/2021JD035017

Trapp, R. J, Diffenbaugh, N. S., Brooks, H. E., Baldwin, M. E., Robinson, E. D., & Pal, J. S. (2007). Changes in severe thunderstorm environment frequency during the 21st century caused by anthropogenically enhanced global radiative forcing. *Proceedings of the National Academy of Sciences*, *104*(50), 19719–19723. https://doi.org/10.1073/pnas.0705494104

Trapp, R. J., Diffenbaugh, N. S., & Gluhovsky, A. (2009). Transient response of severe thunderstorm forcing to elevated greenhouse gas concentrations. *Geophysical Research Letters*, *36*(1), L01703. https://doi.org/10.1029/2008GL036203

Woods, M. J. (2021). *Understanding extreme tornado events under future climate change through the pseudo-global warming methodology*. University of Illinois at Urbana-Champaign.

The impact of human-induced climate change on future tornado intensity as revealed through multi-scale modeling

Matthew J. Woods[1]†, Robert J. Trapp[2], and Holly M. Mallinson[3]

[1]Department of Atmospheric Sciences, University of Illinois.

[2]Department of Atmospheric Sciences, University of Illinois.

[3]Department of Atmospheric Sciences, University of Illinois.

Corresponding author: Robert J. Trapp (jtrapp@illinois.edu)

†Current affiliation: National Weather Service, Las Vegas, NV.

Supplementary Material

Tornado intensification results from vortex stretching, which is dynamically equivalent to conservation of circulation Γ. For an axisymmetric vortex with a uniform core of vorticity on a horizontal plane, circulation is

$$\Gamma = \zeta \pi R^2 \qquad (1)$$

where R is vortex-core radius, and ζ is the vertical component of the vorticity vector. For such an axisymmetric vortex, we can also write:

$$\Gamma = 2\pi R V \qquad (2)$$

where V is the tangential speed of the vortex at radius R. Using (1) and (2), the vertical vorticity of the vortex can thus be expressed as:

$$\zeta = 2V/R \qquad (3)$$

Note here that we can obtain Eq. (3) directly by using the definition of vertical vorticity in polar coordinates,

$$\zeta = \frac{1}{r}\frac{\partial (r u_\theta)}{\partial r} - \frac{1}{r}\frac{\partial u_r}{\partial \theta} \qquad (4)$$

and then substituting $u_r = 0, u_\theta = V\,r/R$, where u_θ and u_r are the tangential and radial velocity components, respectively.

If we evaluate Eq. (3) with $R = 100$ m, then for a weak (i.e., EF0), strong (i.e., EF2), and violent (i.e., EF4) tornado, with $V = 30$ m s^{-1}, $V = 50$ m s^{-1}, and $V = 75$ m s^{-1}, respectively, we find that $\zeta = 0.6$ s^{-1}, $\zeta = 1.0$ s^{-1}, and $\zeta = 1.5$ s^{-1}. Thus, in an idealized vortex with a fixed core radius, vortex intensity is quantified well by vertical vorticity.

Unsurprisingly, these estimates based on an idealized vortex model are of the same order of magnitude as the 10^0 s^{-1} estimate based on typical scale analysis (e.g., Trapp 2013). In real tornadoes with asymmetric, non-uniform cores observed using discrete data, the magnitude of the calculated vertical vorticity depends on the resolution of the data used in the calculations. As would be the case for extrema of any field represented in discrete data, it is logical to expect that the "true" value of ζ will be reduced in coarsened data. This explains why, for example, Coffer et al. (2017) and Gray and Frame (2021) used vertical vorticity thresholds of 0.3 s^{-1} and 0.15 s^{-1}, respectively, for "tornado-like vortex" (TLV) identification on horizontal grids with 125 m and 250 m spacings. A key point here is that the thresholds in these and many other studies are obtained heuristically.

We can, however, demonstrate support of these heuristic estimates by calculating the vertical vorticity of an idealized tornado on a Cartesian grid with different spacings in x and y, i.e., Δx and Δy. Let:

$$u_\theta = \begin{cases} \frac{Vr}{R}, r \le R \\ \frac{VR}{r}, r > R \end{cases} \quad (5)$$

which models a Rankine vortex with a uniform core of vorticity surrounded by irrotational flow; despite its idealization, Eq. (5) also approximates the rotational flow in real tornadoes to varying degrees (e.g., Wurman & Gill, 2000). For consistency with the discussion above, we initially let $R = 100$ m and $V = 50$ m s^{-1}, and thus per Eq. (3), $\zeta = 1.0$ s^{-1} within the core. The arbitrary domain for our calculations is $0 \le x, y \le 5000$ m, and the vortex is centered at $x_o, y_o = 2500$ m. Upon implementing Eq. (5) using $r = \sqrt{(x - x_o)^2 + (y - y_o)^2}$, the resulting velocity field is transformed into Cartesian coordinates, and then $\zeta (= \partial v/\partial x - \partial u/\partial y)$ is determined using centered finite differencing.

On a grid with $\Delta x = 10$ m $= \Delta y$, which resolves well a 200-m diameter vortex, the calculated maximum vertical vorticity is $\hat{\zeta} = 1.0$ s^{-1}, implying that the tornadic vortex intensity is fully represented (Fig. A). If we coarsen the grid to $\Delta x = 250$ m $= \Delta y$, we no longer resolve the vortex, yet Fig. B still reveals a vortex signature, with $\hat{\zeta} = 0.16$ s^{-1}; notice that this vertical vorticity value is nearly the same as Gray and Frame (2021)'s threshold of 0.15 s^{-1} used for TLV identification in model simulations with 250 m grid spacing. If we further coarsen the grid to $\Delta x = 1000$ m $= \Delta y$, which is the grid spacing used in regional model simulations of this study, a size-exaggerated signature of the vortex continues to exist, with $\hat{\zeta} = 0.008$ s^{-1} (Fig. C). Finally, if we increase the tangential windspeed to $V = 75$ m s^{-1}, we find a size-exaggerated signature of the vortex with a larger calculated vertical vorticity, $\hat{\zeta} = 0.012$ s^{-1} (Fig. D). In other words, the increased intensity of a tornadic vortex is represented on a coarse grid as an increase in maximum vertical vorticity, even though the tornado itself is under-resolved.

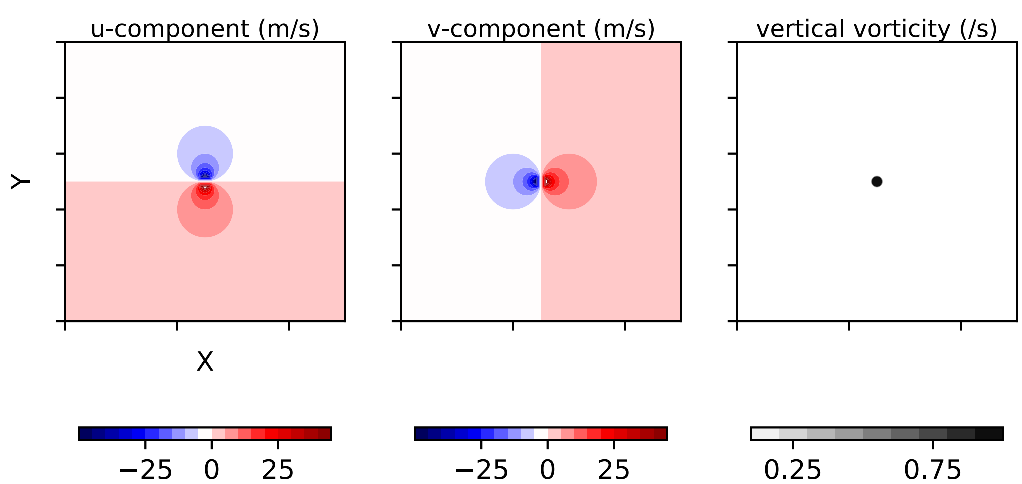

Fig. A. Cartesian component velocities and vertical vorticity for the case $\Delta x = 10$ m, $V = 50$ m s^{-1}, in which $\hat{\zeta} = 1.0$ s^{-1}.

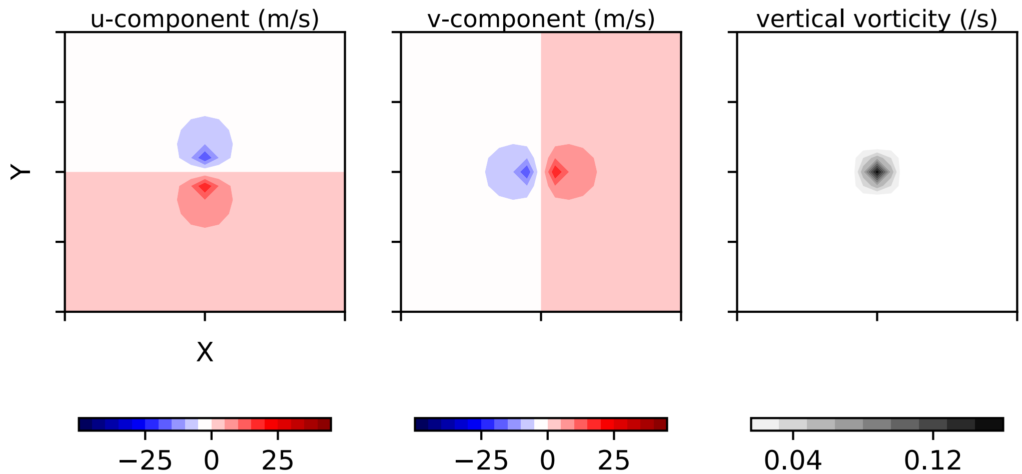

Fig. B. As in Fig. A, except for Cartesian component velocities and vertical vorticity for the case case $\Delta x = 250$ m, $V = 50$ m s^{-1}, in which $\hat{\zeta} = 0.16$ s^{-1}.

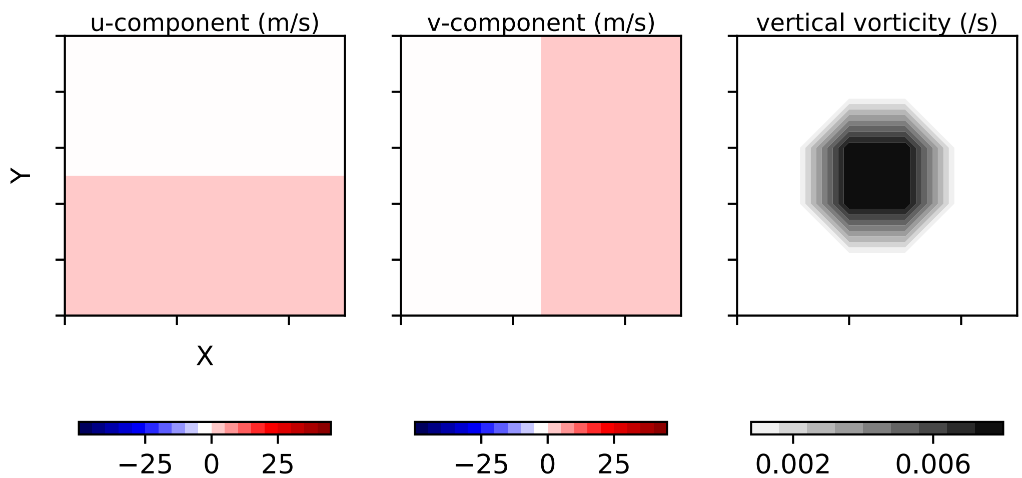

Fig. C. As in Fig. A, except for Cartesian component velocities and vertical vorticity for the case case $\Delta x = 1000$ m, $V = 50$ m s^{-1}, in which $\hat{\zeta} = 0.008$ s^{-1}.

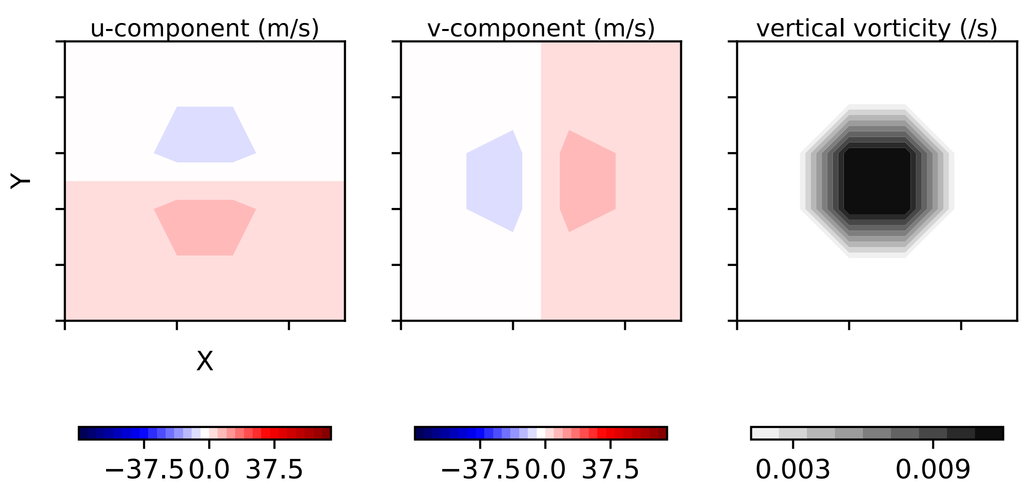

Fig. D. As in Fig. A, except for Cartesian component velocities and vertical vorticity for the case $\Delta x = 1000$ m, $V = 75$ m s^{-1}, in which $\hat{\zeta} = 0.012$ s^{-1}.

The essence of this simple exercise is also revealed in the observational results of Toth et al. (2013; see their section 3), which show high linear correlation between quantifications of tornado intensity (differential velocity) obtained near the surface with high-resolution mobile radar and quantifications of the corresponding tornadic-vortex/mesocyclone intensity determined using the coarser-resolution measurements of the nearest WSR-88D. To be clear, the vortex sampled by a WSR-88D represents some combination of the tornado and its ambient circulation. The essence of the exercise is also reflected in the ongoing efforts to estimate tornado intensity–as manifest by degree of damage, and represented through an EF rating–using radar-quantified characteristics of the mesocyclone or tornadic vortex (e.g., Smith et al. 2020).

Thus, as justified by observational data as well as by analyses of a discretized vortex model, we use magnitudes of vertical vorticity as potential tornado proxies in our regional model simulations with 1-km grid spacings. The vertical vorticity is evaluated at a height of 80 m, which is approximately the height of the first model level above the lower model boundary. Consistent with the vortex-model analysis results, a vertical vorticity value locally exceeding 0.0075 s^{-1}, which is the 99th percentile of gridpoint values in the CTRL simulation, serves as a tornado proxy occurrence. A vertical vorticity value exceeding 0.0125 s^{-1}, which is the 99.9th percentile, serves as a significant tornado proxy occurrence. Coexistence of local updraft velocities exceeding 5 m s^{-1} is required.

References

Coffer, B. E., Parker, M. D., Dahl, J. M. L., Wicker, L. J., & Clark, A. J. (2017). Volatility of tornadogenesis: An ensemble of simulated nontornadic and tornadic supercells in VORTEX2 environments. Monthly Weather Review, 145, 4605-4625, https://doi.org/10.1175/MWR-D-17-0152.1.

Gray, K., & Frame, J. (2021). The impact of midlevel shear orientation on the longevity of and downdraft location and tornado-like vortex formation within simulated supercells. *Monthly Weather Review*, 149, 3739-3759, https://doi.org/10.1175/MWR-D-21-0085.1

Smith, B. T., Thompson, R. L., Speheger, D. A., Dean, A. R., Karstens, C. D., & Anderson-Frey, A. K. (2020). WSR-88D Tornado Intensity Estimates. Part II: Real-Time Applications to Tornado Warning Time Scales. *Weather and Forecasting*, 35, 2493–2506, https://doi.org/10.1175/WAF-D-20-0011.1.

Trapp, R. J. (2013). *Mesoscale-Convective Processes in the Atmosphere*. Cambridge University Press.

Wurman, J., & Gill, S. (2000). Finescale Radar Observations of the Dimmitt, Texas (2 June 1995), Tornado. *Monthly Weather Review*, 128, 2135–2164, https://doi.org/10.1175/1520-0493(2000)128<2135:FROOTD>2.0.CO;2

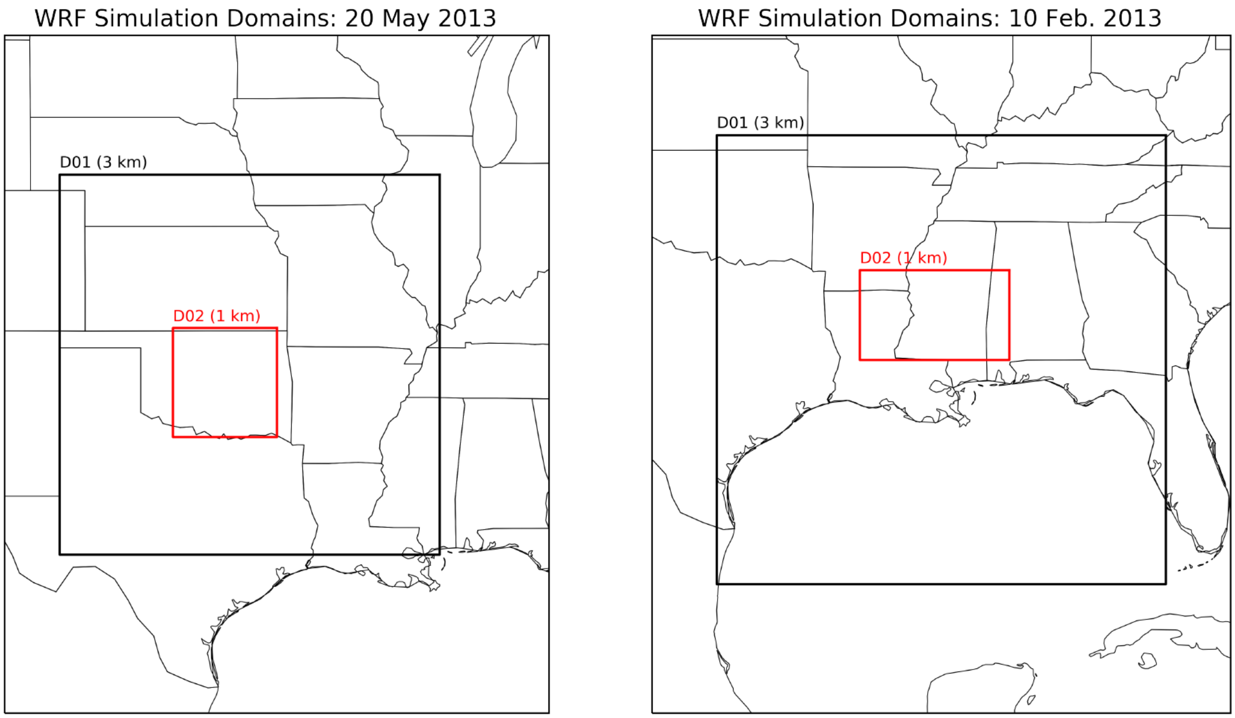

Supplemental Figure S1. Computational domains used for the regional model (WRF) simulations of the 20 May 2013 (WARM) and 10 February 2013 (COOL) events.

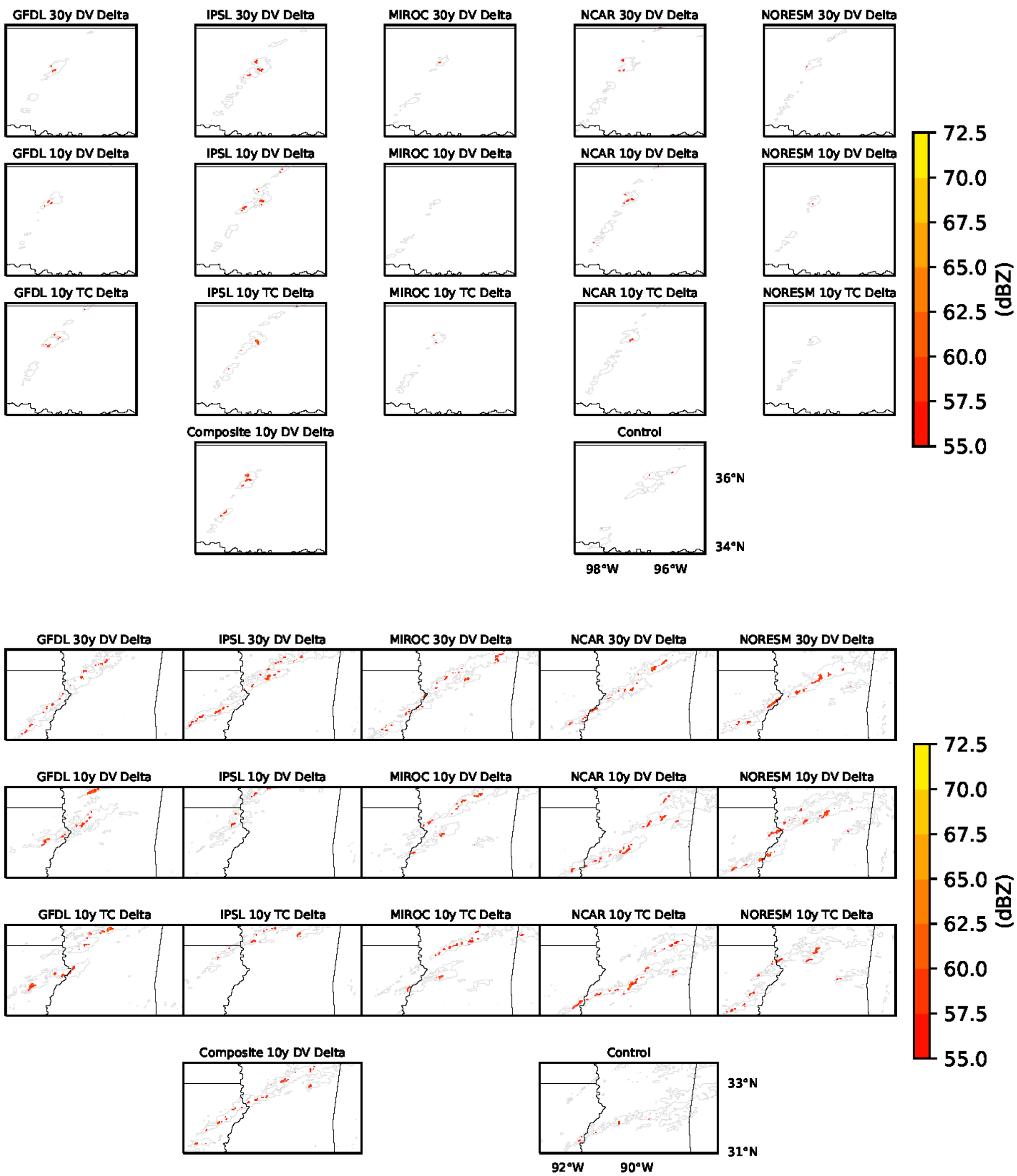

Supplemental Figure S2. Simulated radar reflectivity (dBZ) for the regional-modeling simulations of the WARM event (top panel; 2100 UTC) and COOL event (bottom panel; 0000 UTC). The color fill indicates the areas of intense convective storms over a given simulation. The gray contours are of 30 dBZ radar reflectivity, and show the outline of the convective storms. Each subpanel represents an individual experiment composing the ensemble. See section 2 for guidance on experiment nomenclature.

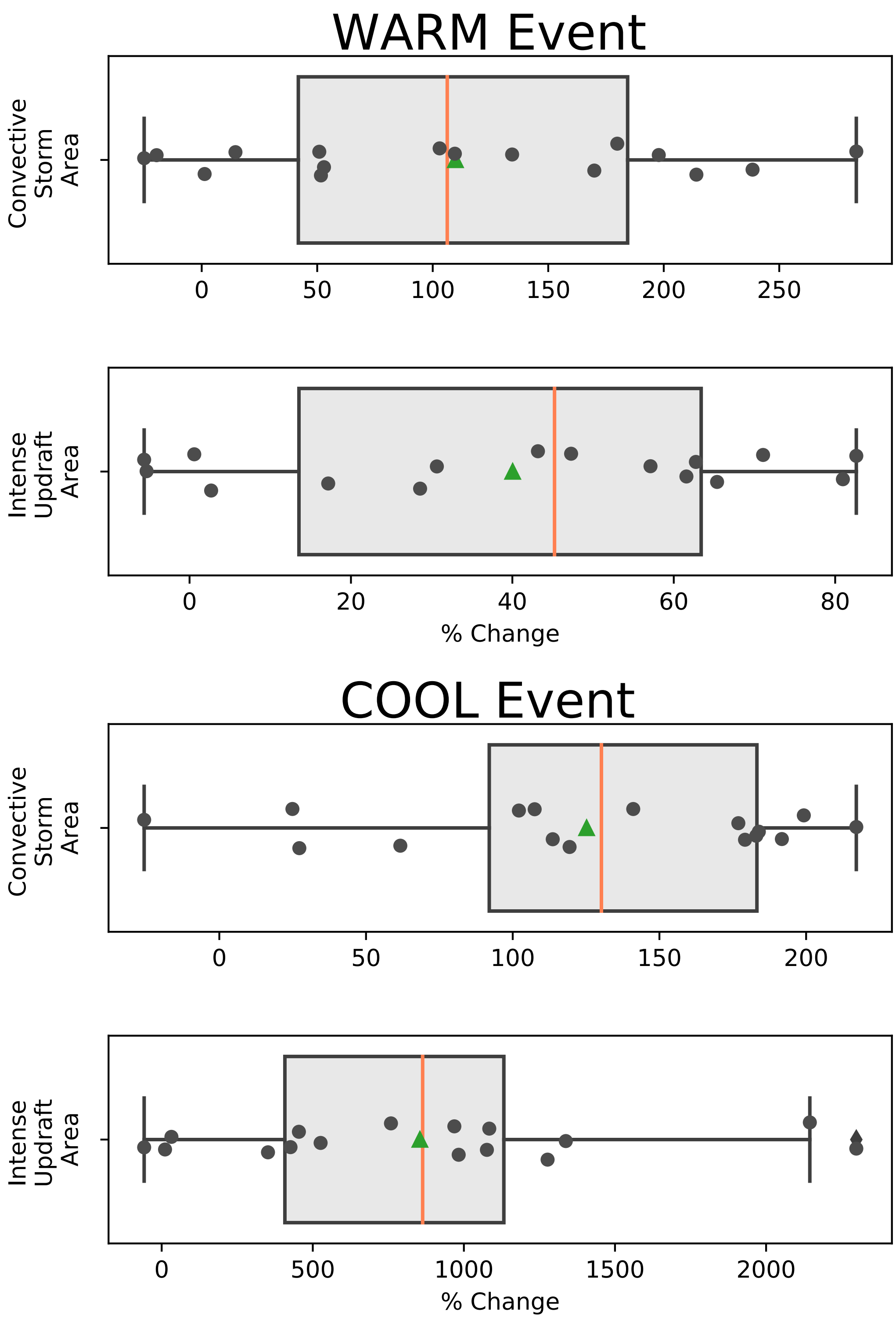

Supplemental Figure S3. Box-and-whisker plots of tornadic-storm intensity-coverage metrics, as evaluated from the regional modeling simulations of the WARM event (top) and COOL event (bottom). Values of these metrics are given as percentage changes in the PGW simulations relative to the control (CTRL) simulation. The median is the orange line, mean is the green triangle, and individual data points are the black circles.

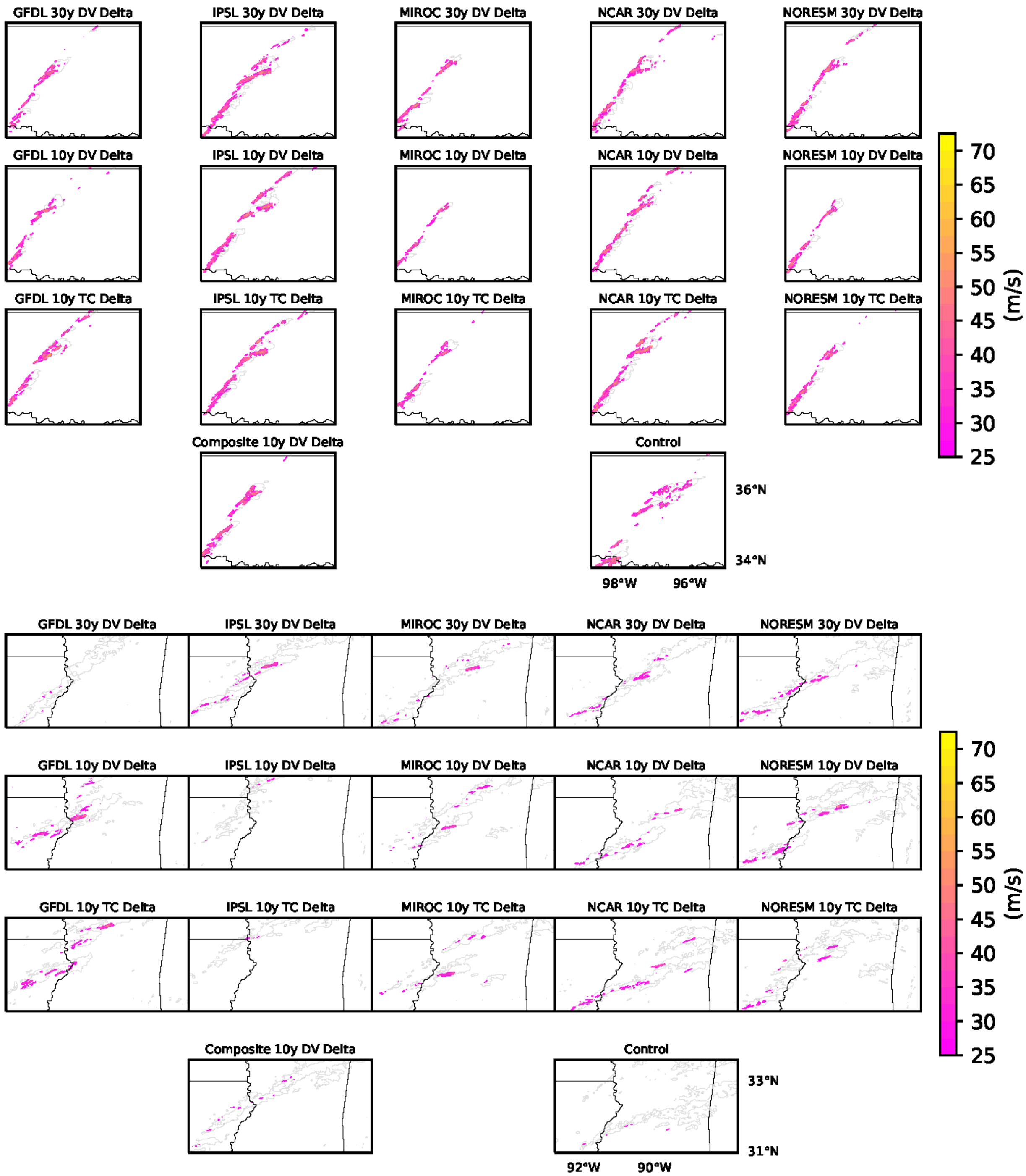

Supplemental Figure S4. Maximum vertical velocity (m/s) for the regional-modeling simulations of the WARM event (top panel; 2100 UTC) and COOL event (bottom panel; 0000 UTC). The color fill indicates the areas of intense updrafts over a given simulation. The gray contours are of 30 dBZ radar reflectivity, and show the outline of the convective storms. Each subpanel represents an individual experiment composing the ensemble. See section 2 for guidance on experiment nomenclature.

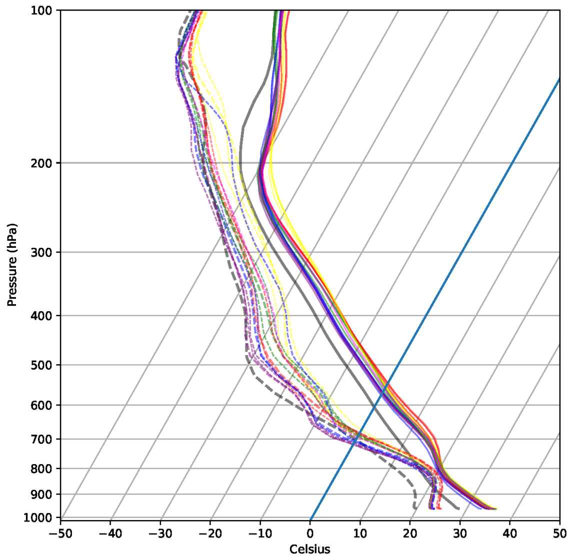

Supplemental Figure S5. Initial and boundary conditions of temperature and dewpoint (°C) for the idealized modeling simulations, for the WARM event (left panel) and COOL event (right panel), as presented on skew-T/log-p diagrams. The solid and dashed black (colored) lines are the temperature and dewpoint for the CTRL (PGW) simulations.

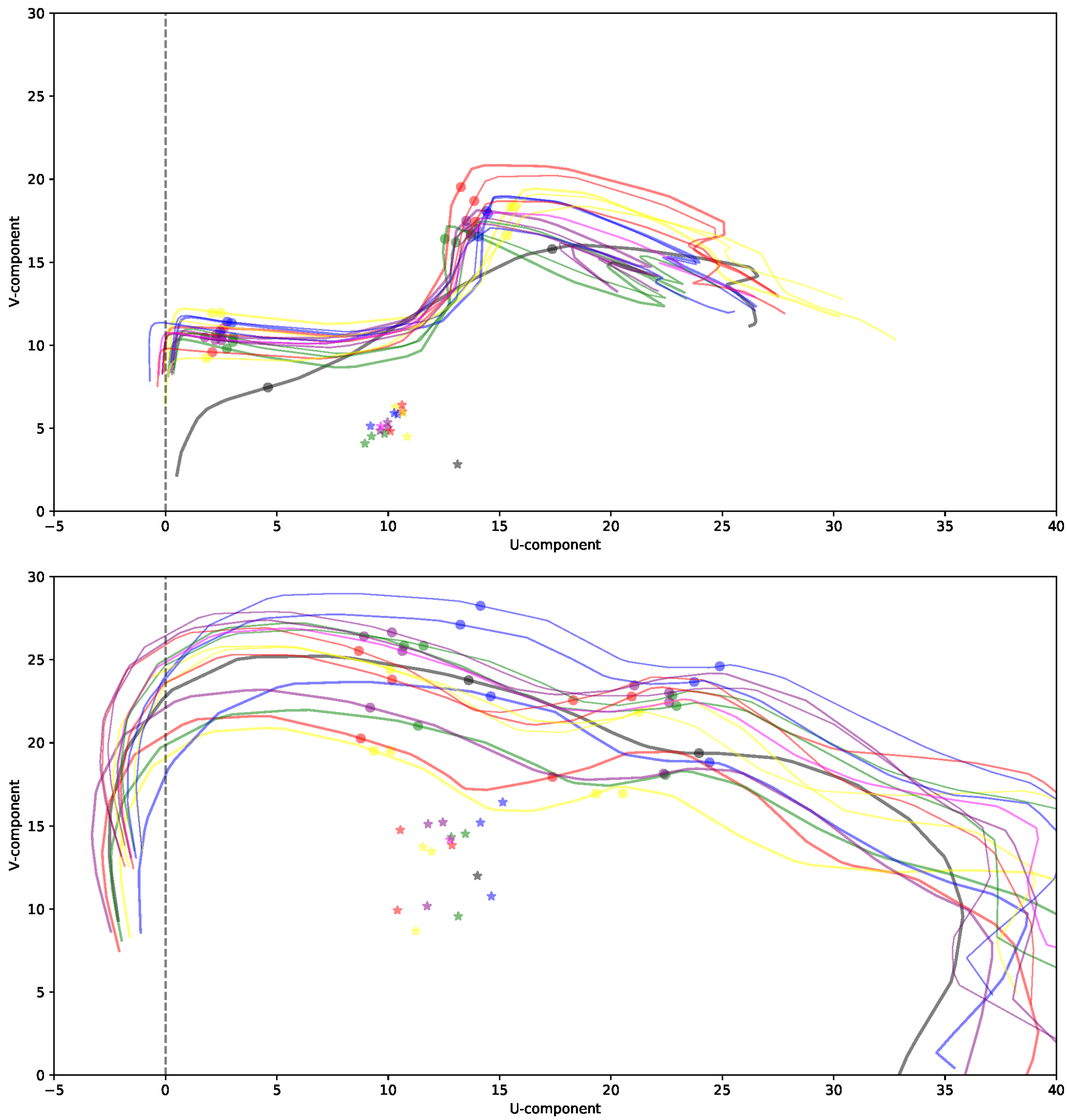

Supplemental Figure S6. Initial and boundary conditions of horizontal wind components (m/s), for the WARM event (top panel) and COOL event (bottom panel), as presented on hodograph plots. The solid (colored) lines are for the CTRL (PGW) simulations. Asterisks show estimated storm motion for a right-moving supercell, and closed circles indicate heights of 1 and 3 km.

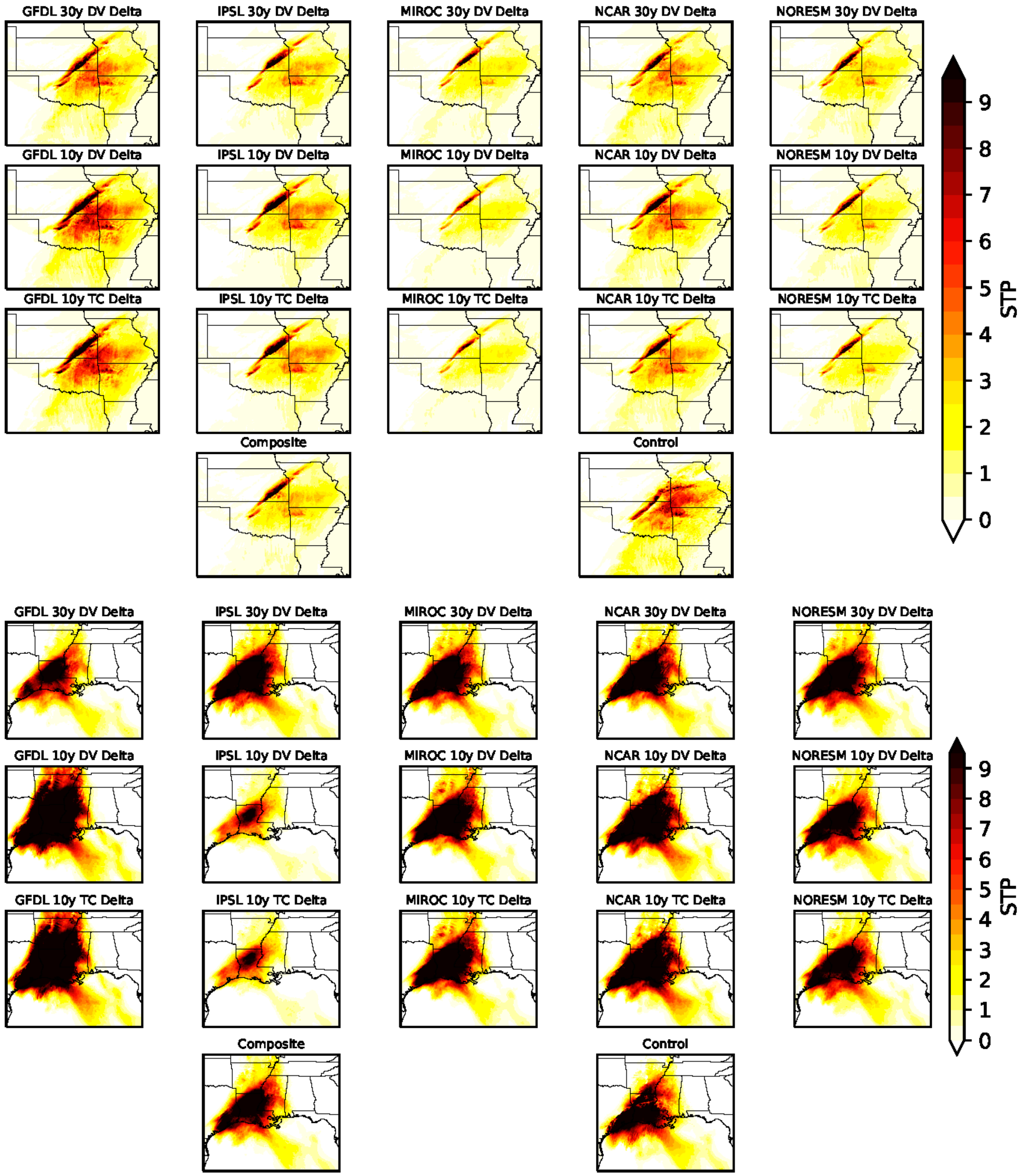

Supplemental Figure S7. Analysis of the significant tornado parameter (STP; nondimensional) over the respective simulation domains (D01; see Fig. S1) of the WARM event (top panel) and COOL event (bottom panel). The calculations were performed using model output at 1800 UTC for the WARM event, and 1500 UTC for the COOL event, which generally represent pre-convective times across the respective simulation domains. See section 2 for guidance on experiment nomenclature.